Multiplicity of K x rays and collective structure in the transitional nuclei with $A \simeq 200$

H. J. Karwowski,* S. E. Vigdor, W. W. Jacobs, S. Kailas,† P. P. Singh, F. Soga,‡
T. G. Throwe, T. E. Ward, D. L. Wark§, and J. Wiggins||
Indiana University Cyclotron Facility, Bloomington, Indiana 47405
(Received 9 November 1981)

The multiplicity $\langle M_K \rangle$ of prompt K x rays emitted in (^{6,7}Li,xn) reactions has been measured for twelve targets in the mass range $180 \leq A \leq 209$, at bombarding energies between 55 and 124 MeV. From the high multiplicities of x rays ($1 \lesssim \langle M_K \rangle \lesssim 3$) characteristic of the observed evaporation residues, we infer that highly converting, low-energy M1 transitions constitute a substantial portion of the γ-decay cascades (especially at moderately high spin, $12 \lesssim I \lesssim 20$) in a large number of nuclides in the transitional region between the shell closure at $N = 126$ and the strongly deformed rare earths. The unexpectedly simple systematic variation of the $\langle M_K \rangle$ measurements with neutron number within this mass region suggests that the converting transitions occur predominantly among members of as yet unknown, mildly deformed, high-K, deformation-aligned rotational bands. From the measured values of $\langle M_K \rangle$ and the singles K x ray yields we extract absolute total cross sections for the (Li,xn) reactions. Expected statistical features of the x-ray multiplicity distributions and associated limits on the applicability of the present technique for evaporation-residue cross section determination are discussed.

NUCLEAR REACTIONS: ^{180}Hf, ^{181}Ta, ^{186}W, ^{185,187}Re, ^{194,198}Pt, ^{197}Au, ^{203,205}Tl, ^{208}Pb, ^{209}Bi(^{6,7}Li,xn), $E_{Li} = 55-124$ MeV; enriched targets; measured x-ray–x-ray and x-ray–γ-ray coincidence yields; deduced K x-ray multiplicity and total (Li,xn) cross sections. Origin of x rays accompanying nuclear reactions, multipolarity of converting γ transitions, structure properties of transitional nuclei.

I. INTRODUCTION

There has been considerable recent interest in the mechanism for the production of prompt x rays accompanying nuclear reactions.[1–9] The yields of such x rays reflect nuclear reaction cross sections and hence are generally smaller by orders of magnitude than the yields of x rays characteristic of the target (or projectile) element, which are copiously produced in charged-particle bombardment via long-range atomic collisions. Two basic classes of mechanism have been discussed for the ionization of inner atomic shells in nuclear reaction products. The first involves electron collisions or rearrangements occurring at some point along trajectories which lead to close approach of the projectile and target nuclei.[5] In the second mechanism the electron vacancies result instead from the decay of excited nuclear states by internal conversion. If the nuclear deexcitation proceeds through a cascade of γ transitions, it is possible for more than one of these transitions to convert, and hence multiple x-ray emission may occur.

X rays from the second mechanism have sometimes been viewed[5] as an undesirable background, masking the small "signal" from atomic collision vacancy-production processes, which might be used, for example, to provide a time calibration for the associated compound nucleus or deeply inelastic nuclear reactions.[5,6,8] In the present work we investigate x-ray emission in fusion-evaporation reactions where internal conversion is the dominant source, and we emphasize that this mechanism itself has a number of interesting and unexpected characteristics and applications.

Our interest in the prompt x rays characteristic of fusion residues was stimulated by the possibility of significant multiple emission per nuclear reaction, as was suggested by a comparison of measured x-ray and γ-ray yields for (α,xn) reactions[9,10] and

also by earlier coincidence studies[11] of fission-fragment x rays from the decay of ^{236}U and ^{252}Cf. We have made direct measurements of the mean multiplicity ($\langle M_K \rangle$) of K x rays emitted from (^{6,7}Li,xn) residues via detection of x-ray−x-ray and x-ray−γ-ray coincidences. As we have reported briefly in previous publications,[12,13] the results of these measurements have been applied both to determine absolute total evaporation-residue production cross sections and to infer certain average properties of nuclear level schemes at moderately high spin in the transitional nuclides with $A \simeq 200$.

The use of the x-ray multiplicity technique to measure total cross sections (σ_{xn}) for (Li,xn) reactions is a crucial aspect of a broader program aimed at understanding the decay modes of hot, high-spin nuclei. The goals and results of that program are reported elsewhere.[14] We developed the present technique since we have concentrated on a mass region where more conventional methods for determining σ_{xn}, involving detection of the heavy residues themselves or of prompt γ-ray spectra from their decay, pose significant experimental problems. In the present paper we apply the x-ray multiplicity technique to fusion residues with $A \simeq 200$ and discuss the expected limits on its usefulness for measuring σ_{xn}. Its success hinges on there being a moderately high multiplicity ($\gtrsim 1$) of K x rays, as we have indeed observed for a large number of bombarding energies and targets in this mass region.

The observation of high $\langle M_K \rangle$ values has in itself interesting implications for the structure of the emitting nuclides, on which we focus in the present paper. We investigate the systematic dependence of $\langle M_K \rangle$ on bombarding energy and on neutron number of the (Li,xn) residues, allowing us to form a consistent picture of the nuclear structure features which may be responsible for the x-ray emission. In particular, we propose that the x rays originate predominantly in highly converting, low-energy $M1$ transitions between states belonging to strongly coupled rotational bands built upon high-K few-quasiparticle intrinsic configurations. We also discuss the general ways in which structure information from $\langle M_K \rangle$ measurements may complement that available from other spectroscopy techniques.

II. METHODS OF DETERMINING X-RAY MULTIPLICITY AND σ_{xn}

In the present experiment we detected characteristic prompt x rays which result from K-shell internal conversion occurring during γ cascades deexciting evaporation residues. During these cascades, transitions proceeding via internal conversion create a vacancy in the atomic K shell. Such a vacancy is filled by an electron from a higher atomic shell very quickly[15]—within $\sim 10^{-17}$ s, with the accompanying emission of an x ray characteristic of $Z_{CN} = Z_{\text{target}} + Z_{\text{projectile}}$. Repeated K-shell conversion (hence multiple K x-ray emission) is then possible since nuclear transition lifetimes for heavy atoms are typically much longer than the atomic vacancy lifetimes.

Our aim is to determine both the absolute total cross section σ_{xn} for producing nuclides with atomic number Z_{CN} and the mean number $\langle M_K \rangle$ of K x rays emitted during the deexcitation cascades in those nuclides. The singles yield N_1 of relevant K x rays in a detector of efficiency η_1 depends on both σ_{xn} and $\langle M_K \rangle$:

$$N_1 = C\sigma_{xn}\langle M_K \rangle \eta_1 , \tag{1}$$

where C is a constant depending on the number of incident particles, the target thickness, dead-time corrections, etc.; σ_{xn} represents the total (particle, xn) reaction cross section summed over all x values; and $\langle M_K \rangle$ is the mean K x-ray multiplicity, an appropriately weighted average over *all* γ-decay paths in *all* (particle, xn) residues.

Two independent techniques have been used in the present work to supplement the x-ray singles measurements in order to extract both $\langle M_K \rangle$ and σ_{xn}. The first technique involves measurement of x-ray−x-ray coincidences and the second, more direct, but much more time-consuming, method is based on detecting coincidences between K x rays and characteristic γ-rays from the accompanying cascades.

In the first method, used for the majority of measurements reported here, the number N_{12} of detected K x-ray−K x-ray coincidences is given by

$$N_{12} = C\sigma_{xn}(\langle M_K(M_K-1) \rangle)\eta_1\eta_2 , \tag{2}$$

where η_2 is the efficiency of the second x-ray detector. Comparison of the singles yield (N_1) with the number N_{12} of coincidences gives

$$D \equiv \frac{N_{12}}{N_1\eta_2} = \frac{\langle M_K(M_K-1) \rangle}{\langle M_K \rangle} = \langle M_K \rangle + \frac{\Delta_K{}^2}{\langle M_K \rangle} - 1 , \tag{3}$$

where $\Delta_K{}^2$ represents the variance ($\langle M_K{}^2 \rangle - \langle M_K \rangle^2$) of the K x-ray multiplicity distribution averaged over all (particle, xn) products. We have extracted values of $\langle M_K \rangle$ from Eq. (3) by assuming a Poisson multiplicity distribution, for which

$\Delta_K{}^2 = \langle M_K \rangle$, and hence

$$D = \langle M_K \rangle \ . \tag{4}$$

Detailed statistical arguments supporting the expected validity of the assumption of a Poisson distribution are given in the Appendix. We argue there that the systematic uncertainty in the extracted $\langle M_K \rangle$ values arising from the possible deviations from a Poisson distribution is not worse than ± 0.2 for the cases we have studied, where we always observe $D \gtrsim 1$.

Once $\langle M_K \rangle$ is known, the total production cross section for (particle, xn) products (σ_{xn}) can be determined from the measured singles x-ray yield at a single angle via formula (1), since the angular distribution of K x rays is isotropic[16] to very good approximation. It is worth noting that the values obtained for σ_{xn} do not depend on the *absolute* values of the x-ray detection efficiency, but only on the ratio η_2/η_1 of efficiencies for the two detectors, which can be determined with better accuracy.

Supplementary measurements of the K x-ray multiplicity were performed in selected cases using the x-ray$-\gamma$-ray coincidence method. These measurements served both as a cross-check on the validity of the x-x coincidence technique and as a source of information about the location of the converting transitions in the level schemes of selected nuclides (see Sec. V A). By comparing the number of coincidences $N_{x-\gamma}$ observed between specific γ rays and K_α and K_β x rays to the number of corresponding γ singles, one obtains directly the mean number $\langle M_K \rangle_\gamma$ of K x rays accompanying the γ transition of interest:

$$\langle M_K \rangle_\gamma = \frac{N_{x-\gamma}}{N_\gamma \eta_x} \ , \tag{5}$$

where η_x represents the efficiency of the x-ray detector. This formula, although similar in form to Eq. (4) for x-ray$-$x-ray coincidences, does *not* depend on the assumption of a Poisson multiplicity distribution. The second moment of the distribution is relevant to the x-x, but not to the x-γ, coincidence yields, because in the former case high-M_K cascades are already weighted more heavily than low-M_K cascades once we detect the *first* of two x rays. There is, however, no such bias introduced when we detect a γ ray. Formula (5) is analogous to the one used in determining γ-ray multiplicity in standard Ge(Li)-NaI coincidence experiments.[17]

Measurements of *triple* coincidences among K x rays have been used to provide another consistency check on the validity of the assumption that the probability of observing a certain number of K x rays in a given (particle, xn) reaction is adequately described by a Poisson distribution with mean value equal to the observed D. In analogy with Eq. (3) the ratio of triple (N_{123}) to double x-ray coincidences is given in general by

$$\frac{N_{123}}{N_{12}\eta_3} = \frac{\langle M_K{}^3 \rangle - \langle M_K{}^2 \rangle}{\langle M_K{}^2 \rangle - \langle M_K \rangle} - 2 \ , \tag{6}$$

where η_3 is the efficiency of the third x-ray detector. If one assumes a Poisson distribution,

$$\langle M_K{}^3 \rangle = \langle M_K \rangle^3 + 3\langle M_K \rangle^2 + \langle M_K \rangle \ , \tag{7}$$

and

$$\langle M_K{}^2 \rangle = \langle M_K \rangle^2 + \langle M_K \rangle \ , \tag{8}$$

from which one obtains, in analogy with Eq. (4),

$$\frac{N_{123}}{N_{12}\eta_3} = \langle M_K \rangle = \frac{N_{12}}{N_1 \eta_2} \ . \tag{9}$$

Therefore, if the assumption of a Poisson distribution of the x-ray multiplicities is valid, one should obtain consistent results for $\langle M_K \rangle$ from the triples-to-doubles and the doubles-to-singles ratios.

III. MEASUREMENTS

A. Experimental configuration

The measurements of K x-ray multiplicity and total (Li,xn) cross sections were made using $^{6,7}Li^{+++}$ beams from the Indiana University Cyclotron Facility. $\langle M_K \rangle$ has been measured for (^{6}Li,xn) reactions at bombarding energies of 55.4, 74.8, 84.4, 94.4, and 124.4 MeV on twelve targets ranging in mass from ^{180}Hf to ^{209}Bi. Measurements for ^{197}Au, ^{208}Pb, and ^{209}Bi targets were also made using ^{7}Li beams of 67.8 and 69.4 MeV. Henceforth we will refer to nominal beam energies: 55, 69, 75, 85, 95, and 124 MeV. The full list of projectile-target-bombarding energy combinations is given in Table I.

The targets (except for ^{186}W and ^{185,187}Re) were made from self-supporting metallic foils of 2$-$10 mg/cm^2 thickness, with isotopic enrichment $>95\%$ in all cases. The W and Re targets were of similar thickness and enrichment, but were made, respectively, from tungsten oxide and from metallic rhenium dissolved in a benzene-styrene solution. The targets were chosen thick enough to stop the heavy evaporation residues yet cause insignificant self-absorption of the low-energy photons of interest.

TABLE I. K x-ray multiplicities, absolute $K_{\alpha 1}(Z_{CN})$ production cross sections, and total (Li,xn) cross sections deduced from x-x coincidence data.

Target	CN	E^{*a}_{CN}	$\bar{N}^b$	$\langle M_K \rangle_x{}^c$	$\sigma_{K_{\alpha 1}}(Z_{CN})$	$\sigma_{xn}{}^d$
			^{6}Li, $E_{lab}=55.4$ MeV			
^{181}Ta	^{187}Os	59.8	106.0	1.08±0.09	575±63[e]	1070±149[e]
^{194}Pt	^{200}Tl	59.5	114.0	2.69±0.17	1054±23	799±83
^{198}Pt	^{204}Tl	61.6	117.8	2.46±0.17	1004±25	832±90
^{197}Au	^{203}Pb	60.8	115.9	1.16±0.09	399±25	702±67
^{208}Pb	^{214}At	48.9	125.0	1.06±0.07	499±36[e]	868±82[e]
			^{6}Li, $E_{lab}=74.8$ MeV			
^{180}Hf	^{186}Re	78.7	104.2	1.56±0.17	1349±216[e]	1729±329[e]
^{181}Ta	^{187}Os	79.3	104.1	1.16±0.26	651±48	1127±265
^{186}W	^{192}Ir	79.0	108.1	2.29±0.17	1353±135[e]	1193±167[e]
^{185}Re	^{191}Pt	78.6	106.2	1.79±0.19	915±110[e]	1086±185[e]
^{187}Re	^{193}Pt	79.9	108.0	1.46±0.15	785±94[e]	1032±175[e]
^{198}Pt	^{204}Tl	81.1	115.9	3.05±0.34	1660±52	1110±127
^{197}Au	^{203}Pb	80.3	114.0	2.15±0.26	688±17	653±81
^{205}Tl	^{211}Po	75.5	120.5	1.82±0.20	913±82[e]	1023±133[e]
^{208}Pb	^{214}At	68.5	123.1	1.70±0.13	875±40	1055±94
^{209}Bi	^{215}Rn	69.8	123.0	2.16±0.20	634±51[e]	605±78[e]
			^{6}Li, $E_{lab}=84.4$ MeV			
^{181}Ta	^{187}Os	88.4	103.4	1.25±0.21	634±61[e]	1023±208[e]
^{194}Pt	^{200}Tl	88.1	111.4	3.12±0.17	1383±88[e]	904±94[e]
^{198}Pt	^{204}Tl	90.2	115.2	3.21±0.16	1627±85[e]	1034±99[e]
^{197}Au	^{203}Pb	89.4	113.3	2.25±0.13	638±37[e]	578±52[e]
^{208}Pb	^{214}At	77.6	122.2	2.24±0.17	786±57[e]	719±67[e]
			^{6}Li, $E_{lab}=94.4$ MeV			
^{181}Ta	^{187}Os	98.2	102.8	1.03±0.25	681±82	1329±360
^{194}Pt	^{200}Tl	98.0	110.8	3.15±0.35	1196±37	775±89
^{198}Pt	^{204}Tl	100.1	114.6	3.21±0.22	1651±35	1049±75
^{197}Au	^{203}Pb	99.3	112.7	1.83±0.29	657±48	732±128
^{203}Tl	^{209}Po	96.4	116.9	1.82±0.38	545±49[e]	614±86[e]
^{208}Pb	^{214}At	87.5	121.6	2.34±0.21	921±29	807±77
			^{6}Li, $E_{lab}=124.4$ MeV			
^{185}Re	^{191}Pt	125.5	102.6	0.80±0.13	521±101[e]	1315±372[e]
^{194}Pt	^{200}Tl	126.1	108.6	2.52±0.26	695±127[e]	563±124[e]
^{198}Pt	^{204}Tl	128.3	112.4	3.13±0.22	1230±216[e]	802±136[e]
^{197}Au	^{203}Pb	127.5	110.5	2.24±0.21	384±66[e]	350±66[e]
^{208}Pb	^{214}At	115.7	119.3	3.09±0.25	518±88[e]	344±62[e]
			^{7}Li, $E_{lab}=67.8$ MeV			
^{197}Au	^{204}Pb	74.3	115.6	2.04±0.13	742±67[f]	742±96[f]

TABLE I. (*Continued.*)

Target	CN	E^{*a}_{CN}	$\bar{N}^b$	$\langle M_K \rangle_x{}^c$	$\sigma_{K_{\alpha 1}}(Z_{CN})$	$\sigma_{xn}{}^d$
			^{7}Li, $E_{lab}=69.4$ MeV			
^{208}Pb	^{215}At	61.6	124.8	1.85±0.15	909±82[f]	1007±120[f]
^{209}Bi	^{216}Rn	63.5	124.6	1.26±0.10	613±55[f]	1002±119[f]

[a]Initial excitation energy of compound nucleus.
[b]Mean neutron number of the populated (Li,xn) residues, determined from γ-singles spectra measured in the present experiment and the work of Ref. 38.
[c]The specified errors in $\langle M_K \rangle_x$ reflect primarily counting statistics and background subtraction uncertainties. Overall absolute normalization uncertainties ($\sim\pm5\%$) and possible systematic errors ($\sim\pm10\%$) arising from deviations from a Poisson x-ray multiplicity distribution are not included.
[d]σ_{xn} is determined from Eq. (11). The quoted errors arise from counting statistics and background subtraction uncertainties in the analysis of x-ray yields, and from uncertainties in the normalization procedure described in Sec. III E of the text.
[e]Absolute x-ray cross sections were obtained via extrapolation or interpolation from the measured energy and Z dependence of the target x-ray production cross sections. Quoted errors include the uncertainty in this procedure.
[f]Absolute x-ray cross sections were obtained via interpolation of the measured energy dependence of the target x-ray production cross sections, assuming (Ref. 22) $\sigma_{^7\mathrm{Li}}(E)=\sigma_{^6\mathrm{Li}}(\frac{6}{7}E)$.

The target chamber and beam transport pipe were constructed from thin (0.8 mm wall) aluminum tubing in order to reduce background and to minimize photon absorption along the path to the detectors.

The detector array consisted of two or three intrinsic germanium crystals of 1 or 1.5 cm thickness and a Ge(Li) detector of 50 cm^3 volume. The detectors were placed at distances from 6 to 15 cm from the target and at laboratory angles of $\pm50°$ and $\pm135°$. The resolution of the primary x-ray detector (Ge 1, with 100 mm^2 active area) was 550 eV (full width at half-maximum) at 100 keV, while the coincidence Ge detectors (Ge 2 and Ge 3, each with 510 mm^2 active area) had $\sim$2.0 keV resolution. The absolute efficiency of the Ge detectors was determined using calibrated standard sources and was almost constant over the x-ray energy range of interest. The efficiency of Ge 1 was typically $\sim1\times10^{-3}$, while the summed efficiency for the two coincidence Ge detectors was typically $\sim5\times10^{-3}$. Iron collimators and thin ($\sim$0.4 mm) Cu absorbers were used to shield all the detectors from low-energy photons present in the room background and to limit the detector singles rates arising from L x rays originating at the target.

Signals from the detectors were processed by conventional electronics which allowed storage of individual time spectra for all relevant combinations of detectors. The time spectra covered a 1 μs range, with typically 15—20 ns resolution for x-ray—x-ray coincidences. High-resolution singles energy spectra from the Ge 1 and Ge(Li) detectors were acquired in multichannel analyzers, while coincidence events were stored event by event on magnetic tape. Good energy resolution was achieved despite the high singles count rates with the help of a pileup rejection system built into the linear amplifiers. Corrections for deadtime and pileup losses in the electronics and computer processing were determined with a pulser fed into the detector preamplifiers and triggered by a scintillator counter viewing energetic particles from the target. The losses were measured independently for the singles and for the coincidence spectra, and were typically $\sim$25% and $\sim$30%, respectively.

B. X-ray singles spectra

X-ray spectra obtained with the high resolution Ge detector during bombardment of ^{187}Re with 75 MeV ^{6}Li and of ^{208}Pb with 69 MeV ^{7}Li are shown in Fig. 1. In addition to the large x-ray peaks resulting from primary ionization of the target element with atomic number Z_t, one observes in each spectrum a series of x-ray peaks characteristic of the nuclear reaction products with atomic numbers Z_t+1, Z_t+2, and $Z_{CN}=Z_t+3$. The x-ray yields accompanying nuclear reactions are surprisingly large in the cases investigated here, being reduced from the atomic collision yields by no more than one order of magnitude. Unfortunately, the $K_{\alpha 2}$

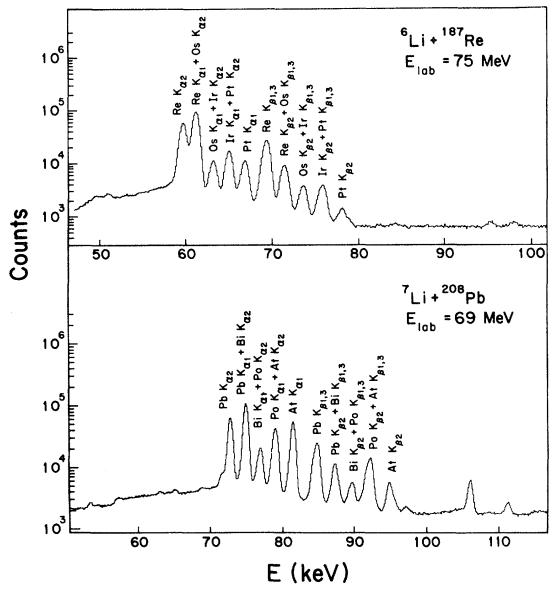

FIG. 1. Representative singles spectra of K x rays from 75 MeV ^{6}Li bombardment of ^{187}Re and 69 MeV ^{7}Li bombardment of ^{208}Pb. Atomic x-ray peaks characteristic of the target element are the strongest in each spectrum. Note that the $K_{\alpha 1}$ and $K_{\beta 2}$ peaks characteristic of Z_{CN} (Pt in the case of the Re target, At for the Pb target) have no contributions from other elements. Unlabeled peaks correspond to low-energy γ rays from reaction products. The energy resolution is the same ($\sim$600 eV FWHM) in the two spectra, but the dispersion of the energy scale differs for the two.

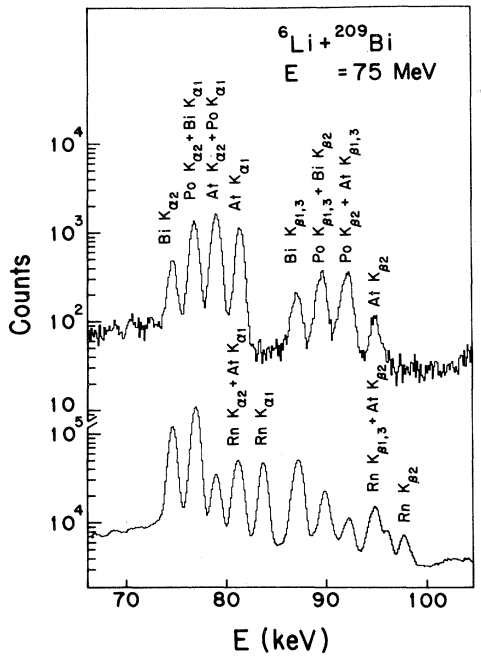

FIG. 2. Representative beam-off singles x-ray spectrum (above) accumulated during a 600 s counting period immediately following $\sim$1 h bombardment of ^{209}Bi by 75 MeV ^{6}Li. The half-lives of the dominant (^{6}Li,xn) residues are 24 and 29 m. A corresponding in-beam spectrum is shown below for comparison. There is clearly no appreciable contribution to the Z_{CN} $K_{\alpha 1}$ and $K_{\beta 2}$ peaks from the β activity of reaction products.

atomic transition energy for each element populated is nearly identical with the $K_{\alpha 1}$ energy from the preceding element, and similarly the $K_{\beta 1,3}$ and $K_{\beta 2}$ peaks from neighboring elements are unresolvable. The only peaks in the spectrum that can be attributed strictly to a single element are the $K_{\alpha 1}$ and $K_{\beta 2}$ peaks characteristic of the compound nucleus Z and the $K_{\alpha 2}$ and $K_{\beta 1,3}$ peaks characteristic of the target Z (if contributions from the element $Z_t - 1$ can be neglected). Besides conversion x rays from evaporation products [(Li,pxn) or (Li,αxn)] the $Z_t + 2$ and $Z_t + 1$ peaks include x rays produced during the deexcitation of residues formed in alpha- or deuteron-transfer reactions, and also considerable contributions from the α or β decay of radioactive (Li,xn) products (half-lives in this region vary from 10 s to 10 h). Despite the fact that the average number of x rays emitted per radioactive decay is generally smaller than the number of prompt x rays per nuclear reaction, the contribution to the observed Z_t, $Z_t + 1$, and $Z_t + 2$ peaks from x rays following α or β decay is not at all negligible. An example of the activity contribution to the in-beam measurements is shown in Fig. 2 by an off-beam spectrum acquired during a 600 s period following $\sim$1 h bombardment of ^{209}Bi. One may note in Fig. 2 the obvious absence of any activity peak in the $K_{\alpha 1}(Z_{CN})$ region. For some of the systems studied we observed small activity contributions (never exceeding 1%) to the Z_{CN} $K_{\alpha 1}$ peak, arising from K_β x rays emitted during the decay of radioactive products with charge Z_t.

There were three primary peaks of interest in the singles spectra: the $K_{\alpha 2}$ and $K_{\beta 1,3}$ peaks characteristic of the target [$K_{\alpha 2}(Z_t)$ and $K_{\beta 1,3}(Z_t)$] and $K_{\alpha 1}$ characteristic of the (Li,xn) residues [$K_{\alpha 1}(Z_{CN})$]. Characteristic target x rays produced in atomic collisions were used to determine absolute K-shell ionization cross sections, whereas the Z_{CN} x rays were applied in determining the cross section and x-ray multiplicity for the (Li,xn) reactions. The $(Z_t + 1)$ and $(Z_t + 2)$ x-ray yields could, of course, also be used in principle to deduce the corresponding residue-production cross sections. We do not present such results here since there is a large uncer-

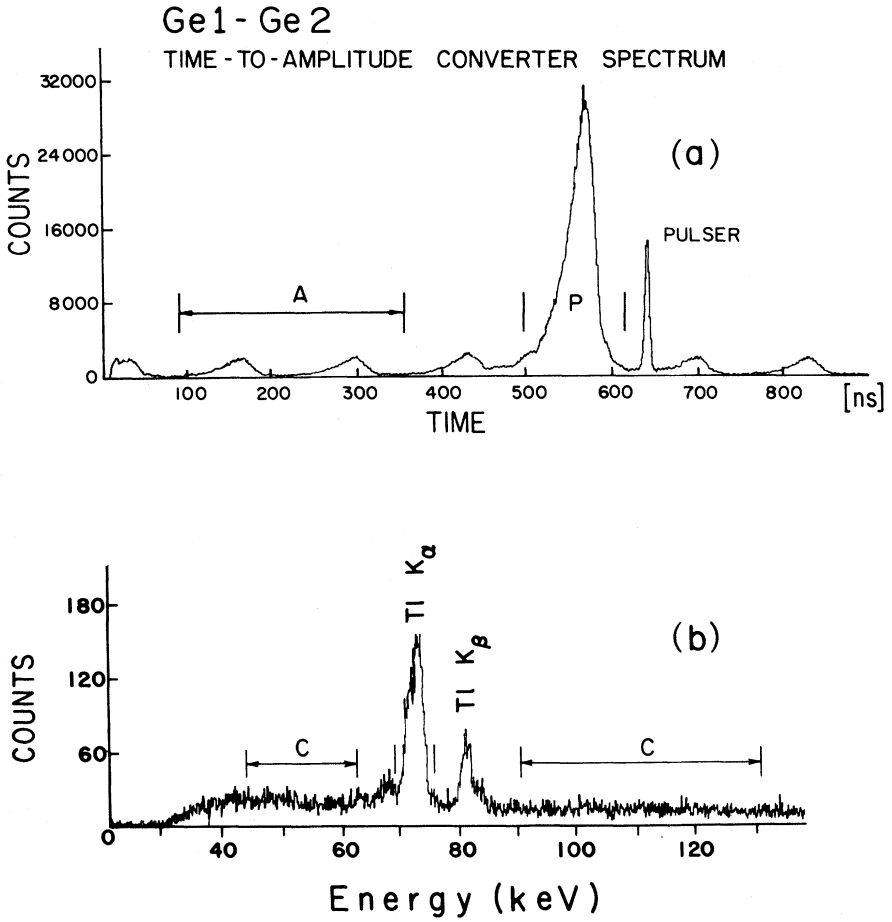

FIG. 3. Representative spectra of (a) the time difference between coincident events in two intrinsic Ge detectors and (b) the energy of events in the poorer-resolution (Ge 2) detector in prompt coincidence with a $K_{\alpha 1}(Z_{CN})$ x ray in the high resolution (Ge 1) counter. The spectra were obtained during 85 MeV ^{6}Li bombardment of ^{194}Pt. The periodic structure in the time spectrum arises from accidental coincidences between events initiated by projectiles from different cyclotron beam bursts. In (b) the Z_{CN} K_α and K_β x ray peaks appear prominently, but the energy resolution of Ge 2 ($\simeq$2.0 keV FWHM) is not sufficient to separate cleanly the constituent K_α or K_β lines. The vertical lines mark the lower and upper edges of (a) the accidental (A) and prompt (P) time windows and (b) the Compton (C) and Z_{CN} K_α energy windows used to gate the Ge 1 energy spectra shown in Fig. 4. Compton background windows on both the low- and high-energy sides of the K x-ray peaks in (b) were used in the sorting process.

tainty in their interpretation, arising from the unfolding of the contributions to the x-ray peaks from neighboring elements, from the subtraction of β-activity contributions, and from the competing nuclear reaction paths which populate these nuclides.

The major uncertainty in extracting the number of counts to be included in the x-ray peaks of interest arises from the background subtraction. In the case of the $K_{\alpha 1}(Z_{CN})$ peak, the background was from 10% to 25% as large as the peak area itself. Smooth backgrounds were drawn under the entire K x-ray region, in a consistent manner for the various targets and bombarding energies, and were subjected to the constraint that the resulting K_α/K_β intensity ratios for both Z_t and Z_{CN} be close to the theoretically expected values.[18] The systematic uncertainty in this subtraction procedure [typically 5—10% of the extracted $K_{\alpha 1}(Z_{CN})$ sum] was estimated by scaling the optimum background curve up and down to the extreme values deemed consistent with the above constraints.

C. X-ray—x-ray coincidence measurements

A representative time spectrum for coincidences between photons in two of the three intrinsic Ge detectors is shown in Fig. 3(a). The corresponding

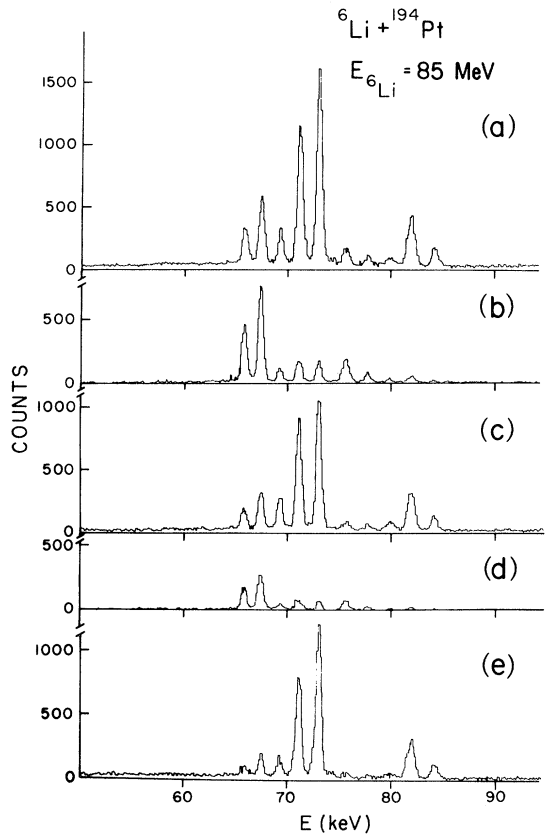

FIG. 4. X-ray spectra for the high-resolution (Ge 1) detector obtained under various Ge 1-Ge 2 coincidence gating conditions, to illustrate stages in the extraction of a true prompt K x-ray$-K$ x-ray coincidence spectrum. The time [accidental (A) or prompt (P)] and Ge 2 energy [Compton (C) or K_α] windows used to gate each spectrum are as follows (see Fig. 3 for the settings of the windows): (a) $P+K_\alpha$; (b) $A+K_\alpha$; (c) $P+C$; (d) $A+C$. Spectrum (e) is the final true prompt coincidence spectrum, obtained by first normalizing the background spectra (b), (c), and (d) to the same time- and energy-window widths as used in (a), and then subtracting the renormalized spectra (b) and (c)$-$(d) from (a).

energy spectrum of Ge 2 events in prompt coincidence with a $K_{\alpha 1}(Z_{CN})$ x ray in Ge 1 is displayed in Fig. 3(b). With this coincidence requirement we observe only K_α and K_β peaks characteristic of Z_{CN} in Fig. 3(b). However, in an ungated Ge 2 spectrum, the Z_{CN} K_α energy window indicated in Fig. 3(b) would also include some contributions from elements of lower Z, because of the limited resolution of this detector. The coincidence spectrum of the high-resolution detector, gated by software windows on the prompt time peak in Fig. 3(a) and on the Z_{CN} K_α energy peak in Fig. 3(b), is shown in Fig. 4(a). The other spectra in Fig. 4 illustrate various types of backgrounds which must be subtracted to generate a spectrum of true prompt K x-ray$-K$ x-ray coincidences, as described below.

There are two primary sources of background in the raw coincidence spectrum of Fig. 4(a). The first originates from accidental coincidences with K_α x rays in Ge 2, and is characterized by the spectrum shown in Fig. 4(b), obtained by shifting the software gate on the time spectrum off the prompt peak, as indicated in Fig. 3(a). The second source corresponds to true prompt coincidences not with real K_α x rays detected in Ge 2, but rather with Compton-scattered γ rays giving pulse-height signals in the same energy range as the K_α x rays. The Ge 1 spectrum in prompt coincidence with the Ge 2 Compton background regions indicated in Fig. 3(b) is shown in Fig. 4(c), and the corresponding spectrum of accidental coincidences with Compton background events is shown in Fig. 4(d). Coincidences of the latter sort are included in both Figs. 4(b) and 4(c), and must be subtracted from one of them to avoid double counting. The *final* coincidence spectrum in Fig. 4(e) is obtained by first normalizing the various background spectra to the same energy- and time-window widths as were used to gate the raw spectrum [Fig. 4(a)], and then subtracting the renormalized spectra b and (c-d) from spectrum a. This background subtraction procedure was followed for all detector combinations of interest.

The number of true prompt $K_{\alpha 1}-K_\alpha$ coincidences $N_{12}(K_\alpha)$ is now obtained by summing the counts in the $K_{\alpha 1}(Z_{CN})$ peak above the low, flat background observed in Fig. 4(e). The uncertainties in $N_{12}(K_\alpha)$ are dominated by counting statistics in the $K_{\alpha 1}$ peaks of the constituent spectra [4(a)$-$4(d)] used in generating the final coincidence spectrum. In extracting a full K x-ray multiplicity value from Eqs. (3) and (4), we must compare the $K_{\alpha 1}(Z_{CN})$ singles yield to the total number (N_{12}) of $K_{\alpha 1}-K_\alpha$ *plus* $K_{\alpha 1}-K_\beta$ coincidences. The latter coincidences were not usually included in the sorting process because the K_β peak-to-Compton ratio in the Ge 2 and Ge 3 spectra were generally poor [see Fig. 3(b)]. However, $N_{12}(K_\alpha)$ can be readily corrected for this omission as follows:

$$N_{12}=N_{12}(K_\alpha)(1+I_\beta/I_\alpha)\,, \tag{10}$$

where the K_β-to-K_α intensity ratio I_β/I_α is taken from atomic physics calculations in Ref. 18, and is $\simeq$0.28 in the Z range of interest. We do not include in N_{12} those events for which one of the K vacan-

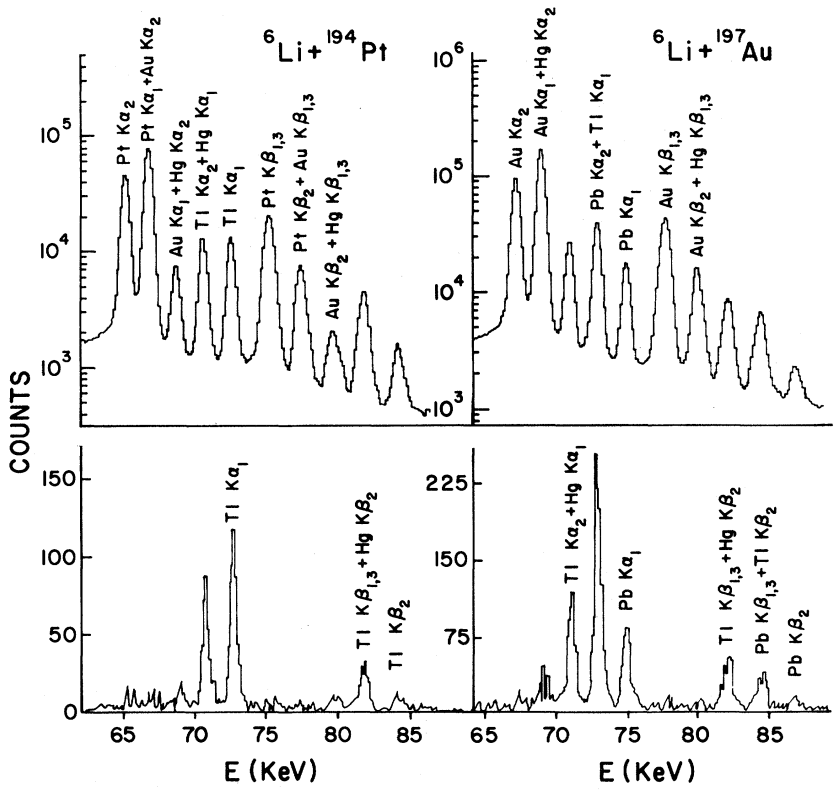

FIG. 5. Singles (top) and true prompt coincidence (bottom) spectra of K x rays from 95 MeV ^{6}Li bombardment of ^{194}Pt and ^{197}Au. The bottom spectra correspond to the background-subtracted final spectrum in Fig. 4(e). The large difference between the two coincidence spectra in the intensity ratio of Z_t+2 to Z_{CN} K x rays is discussed in Sec. V B of the text.

cies is filled in an Auger, rather than a radiative, transition (as occurs $\sim 4\%$ of the time in the elements studied). Thus, $\langle M_K \rangle$ deduced from Eq. (4) is to be interpreted strictly as the multiplicity of K *x rays,* rather than of K-shell *vacancies,* produced in the (Li,*xn*) process.

Further examples of singles and coincidence x-ray spectra, for ^{194}Pt and ^{197}Au at 95 MeV ^{6}Li bombarding energy, are shown in Fig. 5. One may notice that the background under the $K_{\alpha 1}$ (Z_{CN}) peak is much lower in the coincidence than in the singles spectrum. The presence of Z_t+2 peaks in the coincidence spectrum, seen especially strongly for the ^{197}Au target, results from the relatively poor energy resolution in Ge 2 and Ge 3 [i.e., events in these peaks are in coincidence with Z_t+2 K x rays falling within the Ge 2 or Ge 3 K_α gate—see Fig. 3(b)]. The pronounced change in the ratio of Z_t+2 to Z_{CN} x-ray coincidence yields between the Au and Pt targets reflects a difference in multiplicity between even-Z and odd-Z isotopes, which is discussed in Sec. V.

D. X-ray–γ-ray coincidences and x-ray triple coincidences

Coincidence yields between Z_{CN} x rays in the Ge detectors and γ rays in the Ge(Li) detector were measured for 85 MeV ^{6}Li bombardment of ^{198}Pt and ^{197}Au, primarily to check the validity of the x-x method for determining the multiplicity $\langle M_K \rangle$ (see Sec. II). The singles Ge(Li) spectrum for ^{6}Li+^{198}Pt and the corresponding spectrum of γ rays in prompt coincidence with the K_α x rays characteristic of Z_{CN} are shown in Fig. 6. Independent values of $\langle M_K \rangle_\gamma$ [see Eq. (5)] can be obtained in principle from the coincidence-to-singles ratios for each Tl γ line in these spectra, but the complexity of the observed γ spectrum, especially in singles, makes accurate extraction of the multiplicity difficult for all but a few lines.

In contrast, the situation for ^{6}Li+^{197}Au is much cleaner (see Fig. 7) because (1) the singles γ spectrum contains fewer strong lines, and these are more unambiguously identifiable, and (2) the presence of

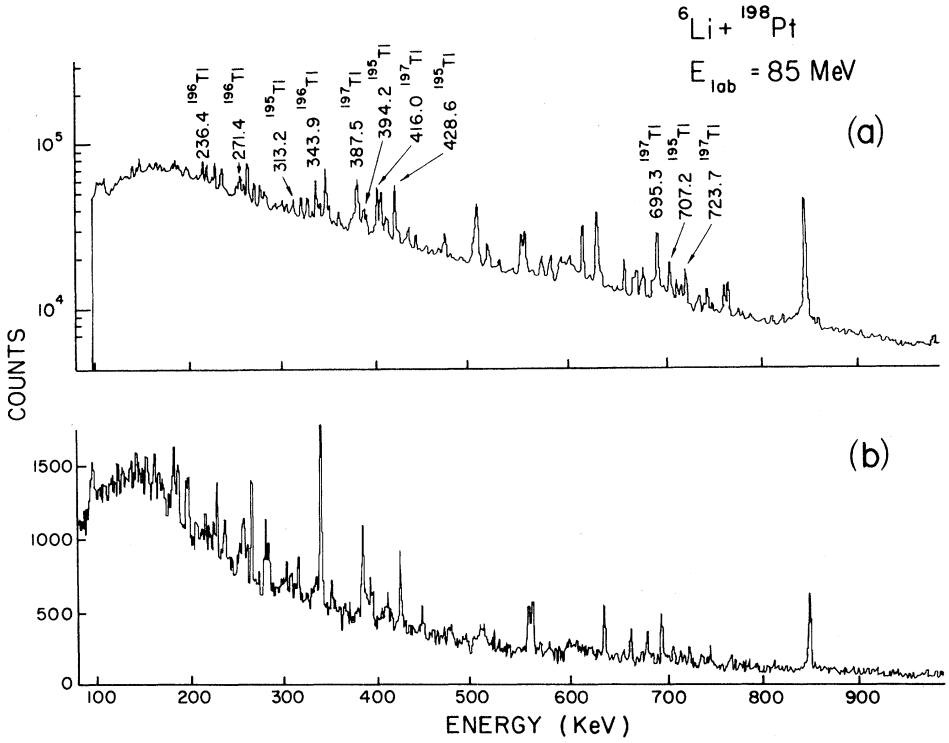

FIG. 6. (a) Singles Ge(Li) spectrum obtained in 85 MeV ^{6}Li bombardment of ^{198}Pt. Only known lines originating from (^{6}Li,xn) reactions are labeled (energies in keV). (b) Spectrum of Ge(Li) events in prompt coincidence with $K_{\alpha}(Z_{CN})$ x ray in any one of three intrinsic Ge detectors.

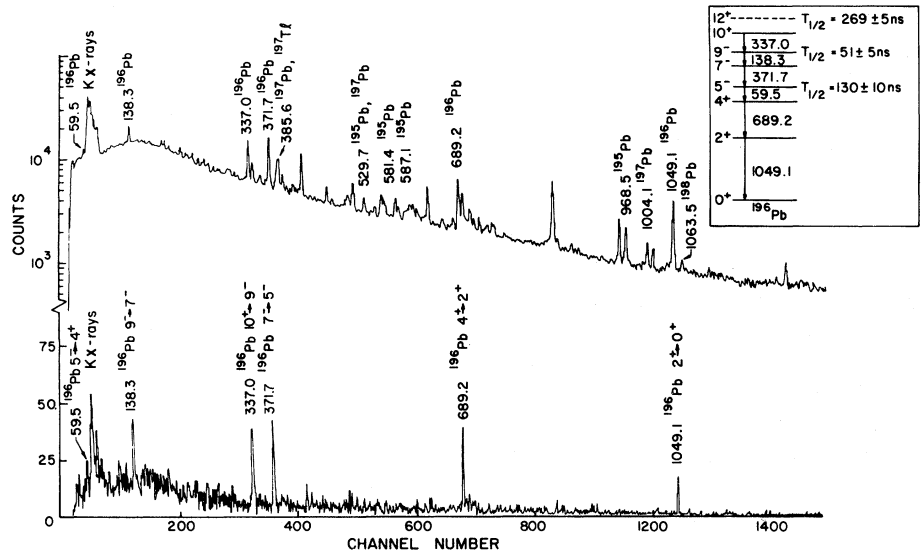

FIG. 7. Top: Singles Ge(Li) spectrum for 85 MeV ^{6}Li+^{197}Au. Only known lines from (^{6}Li,xn) products are labeled (energies in keV). Bottom: Spectrum of Ge(Li) events delayed (by 215—450 ns) with respect to a $K_{\alpha 1}(Z_{CN})$ x ray detected in Ge 1. The transitions depopulating the 12^{+} isomer in ^{196}Pb show up prominently. Inset: Level scheme for the known yrast states in ^{196}Pb.

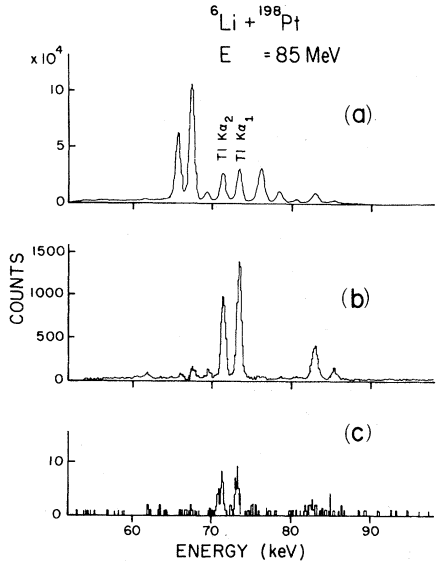

FIG. 8. X-ray spectra for the high resolution (Ge 1) detector obtained for 85 MeV ^{6}Li+^{198}Pt in (a) singles, (b) prompt coincidence with a $K_\alpha(Z_{CN})$ x ray in Ge 2, and (c) prompt three-fold coincidence with $K_\alpha(Z_{CN})$ x rays in Ge 2 and Ge 3. Accidental and Compton background coincidence spectra have been subtracted in obtaining (b) and (c).

high-spin isomers in the decay schemes allows observation of delayed x-γ coincidence spectra dominated by a few prominent lines. For example, in Fig. 7 we show a spectrum of delayed γ rays in coincidence with $K_{\alpha 1}(Z_{CN})$ x rays which are prompt with respect to the cyclotron beam burst. Only γ transitions deexciting the 12^+, $T_{1/2}=269$ ns isomeric state in ^{196}Pb (see inset, Fig. 7) are observed in this coincidence spectrum. Comparison of these delayed coincidence yields with the corresponding singles γ yields allows us to extract (using the known γ-decay lifetimes) the multiplicity of K x rays *feeding* the 12^+ isomer, and hence provides a constraint on the origin of the x rays within the γ decay cascade (see Sec. V A).

For reasons explained in Sec. II, we have also found it useful to acquire triple coincidence yields among Z_{CN} x rays in the three Ge detectors for 85 MeV ^{6}Li bombardment of ^{198}Pt. The spectrum obtained is shown in Fig. 8. Backgrounds from accidental coincidences and from coincidences with Compton-scattered γ rays have been subtracted from the x-ray triples spectrum in Fig. 8 using a procedure similar to that described in the preceding subsection.

E. Absolute normalization procedure

Absolute normalization for the measured x-ray yields was provided in a separate series of runs at bombarding energies of 55 MeV (Pt and Au targets) and 75 and 95 MeV (Ta, Pt, Au, and Pb targets). In these runs singles x-ray spectra were acquired simultaneously with ^{6}Li elastic scattering yields in a 163-cm diameter scattering chamber. The ^{6}Li products were detected in two Si solid state counters placed symmetrically at $10.0°\pm0.04°$ to the left and to the right of the beam direction. The x-ray detector Ge 1 was placed at 120° at a distance $\sim$75 cm from the target. The improved geometry of this experiment in comparison with the coincidence measurements allowed for much smaller background subtraction uncertainties, and hence higher accuracy of the measured x-ray peak intensities.

The absolute x-ray production cross sections were normalized against the ^{6}Li elastic scattering cross sections $[\sigma_{el}(10°)]$ using the measured ratio of x-ray detector efficiency to Si-detector solid angles. The former was determined with a variety of calibrated radioactive sources to an absolute accuracy of $\pm5\%$, while the latter were measured geometrically to $\pm3\%$. In measurements at $E_{^6\mathrm{Li}}=55$ and 75 MeV we took $\sigma_{el}(10°)$ for all targets equal to the Rutherford values (σ_{Ruth}), an assumption accurate to $\sim\pm2\%$ according to optical model calculations.[19] At 95 MeV, values of $\sigma_{el}(10°)/\sigma_{\mathrm{Ruth}}(10°)$ deduced in a previous experiment[14] were used. The absolute target x-ray production cross sections determined via this normalization procedure will be reported elsewhere.[20]

The absolute x-ray cross sections we report at $E_{^6\mathrm{Li}}=85$ and 124 MeV, and for targets other than Ta, Pt, Au, and Pb at all energies, were determined not by direct calibration against the elastic scattering, but rather via interpolation of the absolute target x-ray cross sections $[\sigma_K(Z_t)]$ from the directly measured results at 55, 75, and 95 MeV. In this interpolation procedure, we assumed smooth energy and Z dependences of $\sigma_K(Z_t)$ similar to those measured for α-particle bombardment in corresponding velocity and Z ranges.[10,21]

IV. RESULTS

The K x-ray multiplicities determined from x-ray–x-ray coincidence yields ($\langle M_K\rangle_x$), the measured absolute cross sections for production of $K_{\alpha 1}$ x rays characteristic of $Z_{CN}[\sigma_{K_{\alpha 1}}(Z_{CN})]$ and the to-

tal absolute cross sections for (Li,xn) reactions (σ_{xn}) are listed in Table I, along with a summary of the sources of the quoted uncertainties. We have calculated σ_{xn} from other measured quantities as follows:

$$\sigma_{xn}=\frac{\sigma_{K_{\alpha 1}}(Z_{CN})}{\langle M_K\rangle_x f_{\alpha 1}}\ , \tag{11}$$

where $f_{\alpha 1}$ is the fraction of all Z_{CN} K x rays appearing in the $K_{\alpha 1}$ peak. Values of $f_{\alpha 1}$ were taken from theoretical calculations[18]; for the elements of interest $f_{\alpha 1}$ is typically 0.50. The errors in $\langle M_K\rangle_x$ arise mainly from background subtraction uncertainties in the x-ray singles and coincidence spectra (see Sec. III C) and from coincidence counting statistics. The possible systematic error ($\sim\pm 0.2$) associated with deviations from a Poisson multiplicity distribution (see the Appendix) is not included in Table I. The errors in σ_{xn} reflect those in $\langle M_K\rangle_x$, but include in addition the relative normalization uncertainties for the x-ray cross sections. The variation of $\langle M_K\rangle_x$ with bombarding energy for the five primary targets on which we have made systematic measurements is presented in Fig. 9. A detailed description of these results is given in the next section.

Similar values for $\langle M_K\rangle$ were obtained in the complementary x-γ coincidence experiment. For the two cases investigated in detail, we obtained $\langle M_K\rangle_\gamma=2.37\pm 0.13$ for 85 MeV ^{6}Li bombardment of ^{197}Au and $\langle M_K\rangle_\gamma=3.11\pm 0.30$ for ^{198}Pt bombardment at the same energy. These numbers are cross-section-weighted mean values of $\langle M_K\rangle_\gamma$ averaged over the lowest-lying transitions in various (^{6}Li,xn) residues, and are to be compared with the corresponding $\langle M_K\rangle_x$ values of 2.25 ± 0.13 and 3.21 ± 0.16, respectively. The x-ray multiplicities associated with particular γ transitions are given in Ref. 12.

The excellent agreement between the $\langle M_K\rangle_x$ and $\langle M_K\rangle_\gamma$ values confirms the validity of the x-x coincidence method, and specifically justifies the use of the Poisson x-ray multiplicity distribution. Additional, although weaker, confirmation comes from the x-ray triples measurement for 85 MeV ^{6}Li+^{198}Pt, which yields via Eq. (9) $\langle M_K\rangle_{3x}=3.3\pm 0.6$, to be compared with $\langle M_K\rangle_x=3.21\pm 0.16$.

The measured values of $\langle M_K\rangle_x$ listed in Table I vary from about 0.8 to 3.2, depending on target mass and bombarding energy. This observation agrees qualitatively with a previous determination [involving a comparison of x-ray singles yields with total (α,$xn\gamma$) cross sections] by Deconninck and Longrée[10] of the average number of K-shell vacancies ($\bar{\eta}_K$) produced in α-induced reactions in the same mass region. For incident α energies varying from 40 to 110 MeV, $\bar{\eta}_K$ was observed to increase smoothly from 0.8 to 2.2 for a Pb target and from 0.4 to 1.8 for Bi. In Sec. V A we consider the experimental constraints on the origin of this surprisingly large number of prompt x rays observed. In Sec. V B we explore the systematics of the variation of $\langle M_K\rangle$ with target and energy, and discuss the nuclear structure conditions which may be responsible for this systematic behavior.

The success of the x-x coincidence method, as verified by the complementary x-γ and x-x-x measurements, allows quick ($\sim$1 h per target and bombarding energy) and relatively accurate ($\sim 10-15\%$) measurements of absolute residue-production cross sections, in cases where alternative techniques require either detection of the very low-energy, high-Z residues themselves, or detailed knowledge of γ-decay schemes for products far from the line of stability. The limitations on the x-ray multiplicity method for determining residue cross sections are discussed in Sec. V C and in the Appendix.

The total (Li,xn) cross sections measured in the

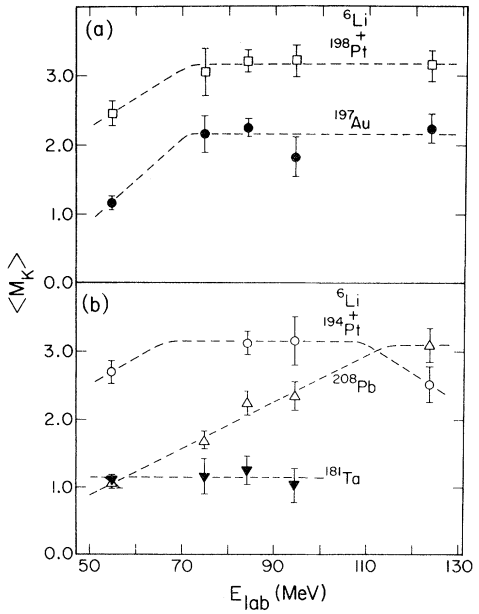

FIG. 9. Measured K x-ray multiplicites for (^{6}Li,xn) reactions on five targets as a function of bombarding energy. The error bars reflect primarily counting statistics and systematic background subtraction uncertainties. The dashed curves are intended to guide the eye.

present experiment constitute a major portion of the total fusion cross sections (σ_{fus}) for the systems studied. Accompanied by measurements of the cross sections for charged-particle evaporation and for fission, these σ_{xn} values have been used in a systematic study of the statistical competition between fission and particle decay modes in heavy-ion fusion products.[14] One may note from the higher energy results in Table I an overall tendency for σ_{xn} to decrease as Z^2/A (i.e., the fissility) of the compound nucleus increases. This behavior is expected because fission competes more favorably with neutron evaporation as fissility increases. Indeed, when the charged-particle emission and fission cross sections are added to σ_{xn}, the measured values of σ_{fus} are found[14] to be essentially independent of target and bombarding energy over the limited ranges covered in the present experiment. The only statistically significant deviations observed from the average value of σ_{fus} are anomalously low results for ^{6}Li+^{197}Au at 75 and 85 MeV. There are no reasons to expect any greater systematic error in our σ_{xn} measurement technique for these cases than for all others; however, we are not confident that the anomaly has a real physical significance.

V. DISCUSSION

A. Constraints on the origin of the x rays

In the present experiment we have observed large yields of K x rays characteristic of nuclear reaction products, specifically $\sim 1-3$ K x rays emitted per (Li,xn) reaction in all the cases studied. The only reasonable mechanism to account for such large yields is internal conversion during the γ cascades deexciting the evaporation residues, although there is no *direct* evidence from our results to verify this claim. In what follows, we argue first that the alternative processes which might in principle lead to production of x rays characteristic of Z_{CN} are expected to be very weak; we then make it plausible that internal conversion can indeed account for not only the observed magnitude of $\langle M_K \rangle$, but also its variation with target and bombarding energy, as long as certain restrictive nuclear structure conditions are satisfied.

The atomic processes capable of producing x rays characteristic of Z_{CN} include: (1) collisionally-induced ionization of a K-shell electron by a Li projectile on its "way in" to fuse with the nucleus of the same target atom; (2) "shakeoff" of a K-shell electron caused by the sudden change of nuclear charge effected by fusion; and (3) K-shell ionization of the fused atom as it recoils through the target foil. One would expect naively that the first process is several orders of magnitude weaker than simple ionization of the *target* (Z_t) K shell, since in the former case impact parameters are restricted to a much smaller range, as the projectile is constrained to undergo subsequent nuclear fusion. Processes (2) and (3) might cause significant rearrangements in outer electron shells, but do not seem likely to produce appreciable K-shell vacancies. These qualitative expectations can be placed on a more quantitative footing on the basis of several measurements and calculations. We note that essentially the same three atomic processes are accessible in α emission from radioactive nuclei. However, in the case of ^{210}Po, they combine to yield a measured daughter-nucleus K-shell ionization probability of only $\sim 2\times 10^{-6}$ per α decay.[23] In a measurement involving relative velocities of the projectile and the K-shell electrons closer to those used in the present experiment, the K-vacancy production probability accompanying compound-nucleus contributions to (p,p') reactions at $E_p=7$ and 12 MeV was determined to be $\sim 10^{-3}$ per nuclear reaction.[8] Calculations of K-shell ionization via "shakeoff" suggest[24] probabilities $\sim 10^{-6}$ per nuclear reaction. Although this information is admittedly fragmentary, it nonetheless indicates that the Z_{CN} x-ray yields observed in the present experiment are too large by several orders of magnitude to arise from the above mentioned atomic processes. This conclusion is also consistent with evidence from x-ray$-\gamma$-ray coincidence measurements for the $\alpha+^{181}$Ta system at $E_\alpha=20$ MeV, where Smolorz *et al.*[2] find that within 8% the observed x-ray yield characteristic of Z_{CN} can be accounted for by internal conversion of known γ-ray transitions in excited residues.

If the Z_{CN} x rays observed in the present experiment arise essentially entirely from internal conversion, what can we say about the nature and location of the converting transitions within the level schemes of the nuclides studied? Experimental constraints on the origin of the K x rays are imposed by: (1) the known low-lying yrast levels in many of the residues populated, (2) our x-γ coincidence data, (3) the total fusion cross sections (σ_{fus}), determined[14] by combining charged-particle measurements with the σ_{xn} values from Table I, and (4) the energy dependence of the $\langle M_K \rangle$ results. This constraining information is most extensive for the neutron-poor Tl and Pb isotopes produced in Li+^{198}Pt, ^{197}Au

bombardment, and for this reason we concentrate on these systems in the discussion below. We will consider the behavior of $\langle M_K \rangle$ for the other targets in depth in the following subsection.

Only a small fraction ($\lesssim 20\%$) of the observed x rays from Pb isotopes formed in ^{197}Au(Li,xn) reactions at the energies studied could be attributed to internal conversion of *known* yrast transitions[25] among states with spin $I \leq 12$. Extensive x-ray side feeding of these low-lying yrast states is unlikely in light of the near constancy in each of several isotopes of the $\langle M_K \rangle_\gamma$ values determined from x-γ coincidence yields for 85 MeV ^{6}Li+^{197}Au (see Ref. 12). Furthermore, coincidence yields between prompt x rays and delayed γ's depopulating the 12^+ 0.27-μsec isomer in ^{196}Pb (see Fig. 7) indicate that all (2.2±0.2 compared to a total of 2.25±0.13) of the ^{196}Pb K x rays observed at 85 MeV bombarding energy result from as yet unknown converting γ transitions which *feed* the 12^+ state. In the Tl isotopes produced in Li+Pt fusion, typically $\sim 0.5-1.0$ of the three x rays observed might arise from known transitions with $I \lesssim 14$ (see Ref. 25 and Sec. V B of the present paper), with the remainder presumably originating again at higher spin.

Information on the upper limit of the spin range of populated states whose decay might be responsible for the observed x rays can be inferred from the measured values of σ_{fus} (900−1300 mb for the Li+Pt, Au systems at all energies[14]). On the basis of σ_{fus} and statistical model calculations[14] (assuming no *lower* cutoff on the entrance-channel orbital angular momenta contributing to fusion) we estimate the average spin at which the (^{6}Li,xn) residues are populated for $E_{^6\text{Li}} = 85$ MeV to be $\langle I \rangle \simeq 20$. As the bombarding energy is lowered to 55 MeV, one would expect this average populated spin to approach $I \simeq 12$, and as a result the x-ray multiplicity to drop off to the smaller values expected from transitions among the known low-spin states. This is indeed observed for both ^{198}Pt and ^{197}Au targets in the low-energy falloff in $\langle M_K \rangle$ shown in Fig. 9(a). We have specific evidence that this falloff is *not* related to the change in neutron excess of the dominant residues between 55 and 75 MeV: A measurement for ^{7}Li+^{197}Au at $E_{\text{lab}} = 69$ MeV, populating the same residues as 55 MeV ^{6}Li+^{197}Au, but at appreciably higher spin, yielded $\langle M_K \rangle = 2.04 \pm 0.16$, in excellent agreement with the higher-energy ^{6}Li+Au results (see Table I).

It thus appears that for all of the Pb and Tl isotopes populated, ~ 2 K x rays must be accounted for by converting transitions in a small region of spin, $12 \lesssim I \lesssim 20$. This condition cannot reasonably be fulfilled if the transitions in this spin region are predominantly $E2$ (of any energy), since the maximum number ($\beta_{K_{\max}}$) of K x rays emitted per E2 transition is 0.14 for $Z = 82$; $\beta_{K_{\max}}$ occurs for $E_\gamma \simeq 150$ keV, below which E2 transitions primarily undergo L-shell and M-shell conversion (see Fig. 10 and Ref. 26). Thus, it would require ~ 14 *optimally* converting E2 transitions to yield ~ 2 x rays. In contrast, low-energy $M1$ transitions are very efficient at producing K x rays in a narrow spin range, because of both their high conversion probability β_K (see Fig. 10) and the small spin change per transition. About five $M1$ transitions of energy $100 \lesssim E_\gamma \lesssim 300$ keV would be sufficient to account for the observed x rays. Contributions to the x-ray

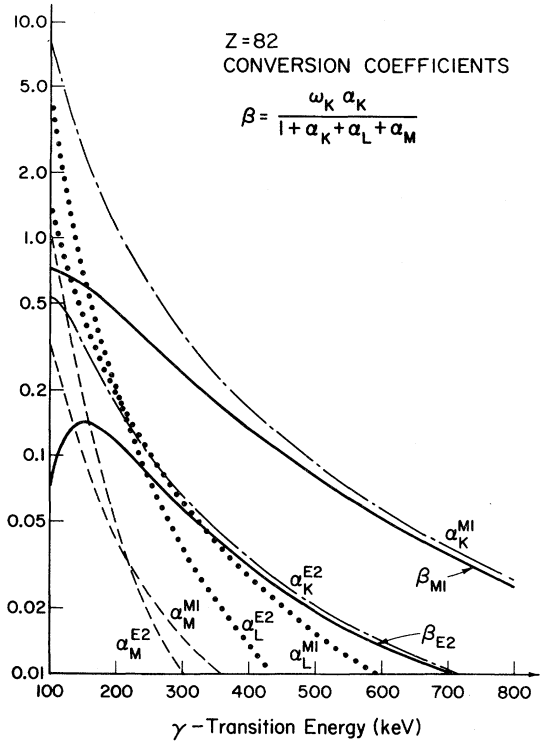

FIG. 10. The coefficients α_K, α_L, and α_M for K-, L-, and M-shell internal conversion of $E2$ and $M1$ transitions in $Z = 82$ nuclei, as a function of transition energy. Also plotted (solid curves) are β_{M1} and β_{E2}, the fraction of all $M1$ and $E2$ transitions which yield K x rays, as calculated from the formula given in the figure, with the K-shell fluorescence factor (fraction of K vacancies filled in radiative atomic transitions) for $Z = 82$ taken to be $\omega_K = 0.968$. The conversion coefficients are taken from Ref. 26.

yield from higher multipolarity transitions (e.g., M2 or M3) are less likely since such transitions tend to have relatively long lifetimes, while the observed x rays are predominantly prompt with respect to the beam, and since too little range in spin is available for a significant number of high ΔI transitions.

In summary, the experimental constraints strongly suggest the existence of a narrow spin range dominated by highly converting low-energy M1 transitions at moderately high spin in the neutron-poor Tl and Pb isotopes, where there is almost no detailed information available about the level schemes. Additional constraints on the nuclear structure in this mass and spin region, provided by the systematic dependence of $\langle M_K \rangle$ on nuclide, will be discussed in the next subsection.

It is useful to consider our x-ray multiplicity results in light of other experimental techniques which have been applied recently to investigate γ-transition multipolarities in continuum or quasicontinuum regions of the photon spectra from high-spin cascades.[27–31] The methods used most extensively involve measurements of γ-ray angular distributions[28–30] or polarization[30,31] and measurements of conversion electron spectra.[32] For example, in ^{161}Yb and ^{174,175}W (Ref. 29), γ-ray anisotropy data suggest the presence of a substantial dipole (E1 or M1) component in the yrast cascades at low transition energies ($\sim$300 keV). On the whole, however, these techniques have so far provided only fragmentary, usually qualitative, and often contradictory (e.g., see Refs. 29–32) evidence regarding the existence of significant M1 contributions to the γ-ray continuum. Although one can deduce information about γ-transition multipolarities from measurements of $\langle M_K \rangle$ only indirectly, the present results nonetheless make it clear that x-ray multiplicity data very usefully complement these other methods. For example, $\langle M_K \rangle$ is very sensitive to the difference between $M1$ and $E1$ transitions, whereas the γ-ray anisotropy is sensitive only to the dipole versus quadrupole nature of the γ transitions. The occurrence of an appreciable admixture of nonstretched radiation in the continuum region can have considerably greater influence on the interpretation of γ-ray polarization and angular correlation experiments[30] than for x-ray measurements.[4] The x-ray multiplicity measurements also complement conversion-electron measurements with respect to the accessible γ-ray energy range: The background-imposed lower limit of γ-ray energy for which singles conversion electron measurements are useful is typically a few hundred keV, whereas the largest contributions to $\langle M_K \rangle$ arise from transitions of 80–400 keV. Some combination of γ-ray, electron, and x-ray measuring techniques applied to the same residual nuclides appears most likely to provide convincing evidence on the multipolarity of high-spin γ transitions.

While evidence independent of our $\langle M_K \rangle$ results concerning the occurrence of $M1$ radiation in the quasicontinuum region is presently inconclusive, it should be stressed that our deduction of an appreciable number of $M1$ transitions in the moderately high-spin γ cascades for $A \simeq 200$ is certainly consistent with available information on discrete low-lying transitions in neutron-poor Tl and Bi isotopes.[33–37] However, the known transitions can account for only a small fraction of the observed x rays. In the following subsection we extrapolate certain features of the known level schemes at low spin to speculate on the nature of the structure at moderate spin responsible for most of the x-ray production.

B. Systematics of $\langle M_K \rangle$ and nuclear structure implications

The $\langle M_K \rangle$ results given in Table I and presented in Fig. 9 exhibit a number of interesting systematic features. In Fig. 9(a), we observe a similar dependence of the multiplicity on bombarding energy for ^{198}Pt(^{6}Li,xn) and ^{197}Au(^{6}Li,xn), with $\langle M_K \rangle$ remaining remarkably constant for each system over the range from 75 to 124 MeV. The significant changes in the mass distribution (from $\sim$6 to $\sim$10 neutrons emitted) and in the spin distribution of the evaporation residues over this bombarding energy range have surprisingly little influence on $\langle M_K \rangle$. The falloff observed in $\langle M_K \rangle$ for both reactions at $E_{\rm lab}=55$ MeV [see Fig. 9(a)] results, as explained in the preceding subsection, from the reduction in spin of the populated residues, rather than from the change in the mass distribution. These results then suggest that the "island" of highly converting transitions at moderately high spin postulated above persists over a relatively long string of Pb and Tl isotopes, without particular regard for the presence of unpaired neutrons. Additional evidence that the isotopic dependence of $\langle M_K \rangle$ is quite weak in this mass region comes from the similarity of the measured multiplicities for the ^{194}Pt and ^{198}Pt targets at $E_{\rm lab}=85$ and 95 MeV (see Table I and Fig. 9), and from the x-γ coincidence measurements, which show[12] that $\langle M_K \rangle$ is equal within experimental un-

certainties ($<20\%$) for neighboring even-A and odd-A Pb or Tl isotopes. Our results are in marked contrast with a recent measurement of K-shell ionization yields per nuclear reaction ($\bar{\eta}_K$) in a number of Dy isotopes formed in α- and ^{12}C-induced reactions.[4] In that experiment $\bar{\eta}_K$ was found to be strongly dependent on the specific nuclide populated, with a pronounced staggering of $\bar{\eta}_K$ (by more than a factor of 2) between adjacent even-A and odd-A isotopes, as one would expect when the x-ray emission is dominated by conversion of relatively few low-lying γ transitions.

While the $\langle M_K \rangle$ results in Fig. 9(a) exhibit little isotopic dependence, they are clearly sensitive to the Z of the compound nucleus: $\langle M_K \rangle$ for Tl residues is systematically higher by about one unit than for neighboring Pb residues. The difference can be accounted for approximately by transitions among known low-spin ($I \lesssim 14$) Tl states. The Z dependence is reflected in the change of the relative intensities of Z_t+2 and Z_{CN} x rays between the two coincidence spectra shown in Fig. 5. Since the coincidence yield depends essentially on $\langle M_K \rangle^2$ [see Eq. (2)], K x rays from Tl residues are considerably enhanced over those from Pb residues in the ^{6}Li+^{197}Au case; in contrast, x rays from Hg are barely observed in the coincidence spectrum for ^{6}Li+^{194}Pt, suggesting again that the multiplicity for even-Z residues is substantially lower than for odd Z.

The different energy dependences of $\langle M_K \rangle$ observed for three other targets in Fig. 9(b) would seem to suggest that the arguments above are applicable only to a quite limited range of nuclides. While $\langle M_K \rangle$ for the ^{194}Pt target is quite similar to the ^{198}Pt results at the lower bombarding energies, it falls off appreciably at 124 MeV. In contrast, $\langle M_K \rangle$ rises steeply with bombarding energy for ^{208}Pb, but is constant and low for ^{181}Ta. It becomes clear that these apparently haphazard energy dependences simply represent different "slices" of a broader systematic behavior when we plot the $\langle M_K \rangle$ results, not against bombarding energy, but rather as a function of the neutron number $\bar{N}$, averaged over the mass distribution of residual nuclides appropriate to each target and energy. This is done in Fig. 11, where we have included all the $\langle M_K \rangle$ measurements from Table I except those for $E_{^6\mathrm{Li}}=55$ MeV, since we have argued in Sec. V A that the 55-MeV results are low for reasons independent of any variation of $\bar{N}$.

The data in Fig. 11 clearly establish the existence of two separate plateaus (for even-Z and for odd-Z compound nuclei) of high and constant $\langle M_K \rangle$ in the region with $110 \lesssim \bar{N} \lesssim 120$. Furthermore, the multiplicity falls off rapidly, and roughly linearly, from both plateaus for $\bar{N} \lesssim 110$ and $\bar{N} \gtrsim 120$. (Henceforth, we drop the distinction between the experimentally determined quantity $\bar{N}$ and the neutron number N.) The results for compound nuclei within a few protons on either side of the $Z=82$ shell closure appear to fall on the same "universal curves." Fluctuations of the measurements about these "universal curves" appear to set in when $\langle M_K \rangle \lesssim 2$, but even then are surprisingly small in light of results for other mass regions.[2,4]

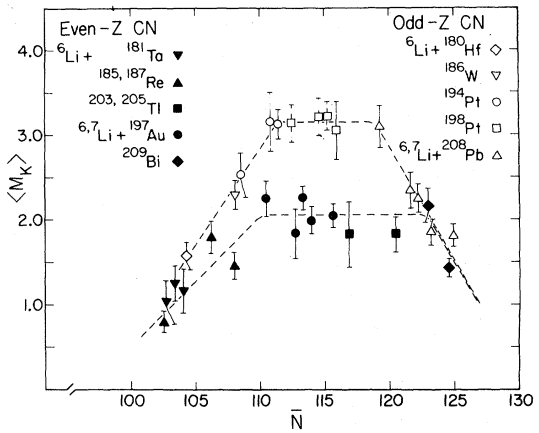

FIG. 11. Compilation of measured K x-ray multiplicities for (Li,xn) reactions induced on the targets shown at bombarding energies from 75 to 124 MeV, plotted versus the neutron number $\bar{N}$ averaged over the residual-nuclide production distribution appropriate to each target and energy. [Typically, two or three (Li,xn) residues are significantly populated for a given target and energy.] The values of $\bar{N}$ are deduced to within ± 0.5 from systematics established by γ-singles spectra measured in the present experiment and the work of Ref. 38. The dashed curves guide the eye and are qualitatively consistent with the nuclear structure arguments presented in the text.

What persistent features of the nuclear structure in the mass region we have investigated are reflected in this simple systematic behavior of $\langle M_K \rangle$? One can construct a scenario qualitatively consistent with all our observations by supposing that at moderately high spin ($I \gtrsim 12$) in the transitional-shape nuclides with $110 \lesssim \bar{N} \lesssim 120$, the γ cascades proceed mainly through strongly coupled (deformation-aligned) rotational bands. We will demonstrate below that if such bands are built upon mildly deformed, high-K, few-quasiparticle [e.g., $(\nu i_{13/2})^2$ or $(\pi h_{9/2})(\nu i_{13/2})$] intrinsic states, then the

intraband γ transitions may optimally satisfy the conditions required for high K-shell conversion probabilities. After these general qualitative considerations, we will discuss the level of support for this scenario from the quantitative information presently available concerning the level schemes in these transitional nuclides.

Adjacent levels within strongly coupled bands differ by one unit of spin, rather than by two units, as is characteristic of weakly coupled bands. The $\Delta I=1$ transitions within such bands have energy

$$E_\gamma(I\to I-1)=\frac{\hbar^2 I}{\mathcal{I}}\ , \tag{12}$$

where $\mathcal{I}$ is the moment of inertia with respect to the rotation axis. Intraband $M1$ transitions compete with nonstretched $(I\to I-1)$ and stretched $(I\to I-2)$ $E2$ transitions, both of which are much less likely to yield K x rays (see Fig. 10). Assuming axial and reflection symmetry for the nucleus,[39] the ratio of leading-order collective $M1$ to $E2$ reduced transition probabilities (for $K\neq\frac{1}{2}$) is given by[40,41]

$$\frac{B(M1;K,I\to K,I-1)}{B(E2;K,I\to K,I')}=\frac{\left[\frac{3}{4\pi}\right]\left[\frac{e\hbar}{2Mc}\right]^2(g_K-g_R)^2K^2\langle IK10\,|\,I-1K\rangle^2}{\left[\frac{5}{16\pi}\right]e^2Q_0{}^2\langle IK20\,|\,I'K\rangle^2}\ , \tag{13}$$

where g_K and g_R are the g factors corresponding, respectively, to the intrinsic and collective rotational components of the total angular momentum. If we express the quadrupole moment Q_0 in barns and the $\Delta I=1$ transition energy E in MeV, then Eq. (13) yields the following ratio of transition rates T for $M1$ vs *nonstretched* $E2$ transitions:

$$\frac{T(M1;K,I\to K,I-1)}{T(E2;K,I\to K,I-1)}\simeq 1.3\frac{(I^2-1)(g_K-g_R)^2}{Q_0{}^2E^2}\ ; \tag{14}$$

the corresponding ratio for $M1$ vs *stretched* $E2$ transitions is given (for $I>>1$) by

$$\frac{T(M1;K,I\to K,I-1)}{T(E2;K,I\to K,I-2)}\simeq 0.16\left[1+\frac{5}{2I}\right]\frac{K^2I^2(g_K-g_R)^2}{(I^2-K^2)Q_0{}^2E^2}\ . \tag{15}$$

Equations (14) and (15) indicate that $M1$ transitions within strongly coupled bands would be enhanced with respect to both stretched and nonstretched $E2$ transitions by the postulated large values of K and I, which are easily accessible in heavy nuclei because of the availability of high-j single-particle orbitals. The small quadrupole moments characteristic of the transitional nuclei (Q_0 decreases from ~ 8 b for rare-earth nuclei of $A\sim 170$ to ~ 4 b in the $A\simeq 190$ region[41]) also tend to increase $T(M1)/T(E2)$. An additional requirement for $M1$ enhancement is a microscopic configuration appropriate to yield a significant difference between g_K and g_R, which is not unusual in this mass region.[33,35,36] Furthermore, despite the mild deformation assumed for the postulated strongly coupled bands, the heavy nuclei considered here have relatively large moments of inertia (rigid sphere moment $\mathcal{I}_{\rm rig}/\hbar^2\sim 100$ MeV^{-1}). The large value of $\mathcal{I}$ yields rotational transition energies [see Eq. (12)] small enough to give large K-shell conversion probabilities for $M1$ decay.[26]

The qualitative considerations of the preceding paragraph may be illustrated by a numerical example. Consider a strongly coupled band with $K=12$ and I ranging from 12 to 22 (essentially the angular momentum "window" discussed in Sec. V A). If the moment of inertia for the band is $0.7\mathcal{I}_{\rm rig}$, then the $\Delta I=1$ transition energies correspondingly vary from ~ 180 to ~ 300 keV. If $Q_0=4$ b and $g_K-g_R=0.4$, both realistic values for this mass region,[33,35] then the $I=22$ state will decay $\sim 79\%$ of the time by an $M1$ transition, $\sim 1\%$ by $\Delta I=1$ $E2$, and $\sim 20\%$ by stretched $E2$. The corresponding decay fractions for $I=14$ are 96% $M1$, 1% nonstretched $E2$, and 3% stretched $E2$. With these values for the decay fractions, use of the conversion probabilities plotted in Fig. 10 yields a total of ~ 3.1 K x rays emitted on the average during a deexcitation cascade from the $I=22$ to the $I=12$

member of the band.

In reality, of course, it is highly unlikely that the decay in any nuclide will proceed 100% of the time through a single, simple band, such as just considered. Nonetheless, the numerical example serves to make it quite plausible that strongly coupled bands at moderately high spin may account in large part for the observed x-ray multiplicities for the transitional nuclides. The unit difference observed in $\langle M_K \rangle$ for even-Z vs odd-Z compound nuclei (see Fig. 11) could be attributed to similar bands at lower spin built, for example, upon an $h_{9/2}$-particle state for the unpaired *proton,* as are known to exist in relevant odd-A Tl (Refs. 33–35) and Bi (Ref. 37) isotopes.

The proposed scenario has the additional advantage of providing a natural framework for understanding the observed behavior of $\langle M_K \rangle$ outside the $100 \leq N \leq 120$ plateau. The rapid falloff in $\langle M_K \rangle$ observed in Fig. 11 for decreasing N would be expected, as we enter the strongly deformed region, where yrast cascades are dominated by collective $E2$ transitions.[27] On the other side of the plateau, in nuclei approaching spherical symmetry at the $N=126$ shell closure, collective rotational bands should disappear, resulting again in a rapid reduction of $\langle M_K \rangle$. One would also expect the systematic difference in $\langle M_K \rangle$ between even- and odd-Z residues, attributed above to rotational bands, to vanish as one approaches the shell closure, and this feature is indeed suggested by the present data for $N \geq 122$.

The high-K bands we have introduced to account for most of the emitted x rays have not yet been directly observed in γ-ray spectroscopic investigations. There is, however, considerable existing information on the decay schemes and multipole mixing ratios in the transitional $A \simeq 200$ region which supports the general idea of widespread strongly coupled band structures with high cumulative K-shell conversion probabilities. For example, such bands based upon the $\frac{9}{2}^-[505]$ Nilsson state originating from the $h_{9/2}$ proton orbit have been found in a number of odd-even Tl and Bi nuclides.[34–37] Indeed, detailed γ-spectroscopy measurements have revealed a large number of $M1$ transitions, with $\lesssim 20\%$ $E2$ admixtures, between members of the $\frac{9}{2}^-$ bands, and also higher-lying positive-parity bands, in ^{195}Tl, ^{197}Tl, and ^{203}Bi.[33,37] Lieder *et al.*[33] have observed a quenching of the energy spacings between $\frac{9}{2}^-$ band members at moderately high spin in odd-even Tl isotopes, which would tend to enhance internal conversion. In all, one may account for ~ 0.6 K x rays coming from conversion of known transitions within the $\frac{9}{2}^-$ bands in ^{195,197}Tl, and ~ 0.9 x rays from known transitions in ^{200}Tl, using measured multipole mixing ratios and intensity ratios for the different transitions.[33,42] In contrast, less than 0.15 x rays can arise from converting transitions among known states in the even-Z Hg and Pb isotopes[25,43] of similar neutron number. The known strongly coupled bands built upon an $h_{9/2}$-particle state for the unpaired proton can thus account well for the observed difference in $\langle M_K \rangle$ between even- and odd-Z residues (see Fig. 11), but not for the overall magnitude of the measured multiplicities.

The observed band structure in the Tl isotopes can be reproduced quite well by a model in which particles are coupled to a rotating, soft triaxial core.[44] In the case of ^{198}Tl, calculations within this model show that a proton in the $h_{9/2}$ Nilsson orbit favors strong coupling while a neutron hole in the $i_{13/2}$ orbit produces decoupled bands (see also Ref. 34). This difference could explain why we observe a substantial change in $\langle M_K \rangle$ between even and odd Z, but no appreciable sensitivity to the presence of an unpaired neutron.

There is little information independent of measured multipole-mixing ratios on the g-factor differences $g_K - g_R$ in the mass region of interest. Both measurements[41] and Nilsson model calculations[45] yield $g_R \sim 0.3$. However, for g_K, which depends sensitively on the intrinsic configuration of the nuclear state,[46] neither direct experimental results nor systematic cranking-model calculations are available for the neutron-poor transitional nuclei. The $g_K - g_R$ values deduced from measured mixing ratios are close to unity for a number of members of the $\frac{9}{2}^-[514]$ band in ^{177}Ta, ^{177,181,183}Re, and ^{189}Au (Ref. 47) and vary from 0.5 to 1.1 for members of negative-parity bands in $^{196-201}$Tl (Refs. 33–35, 42, and 48). Calculations by Toki *et al.*[44] yield $g_K - g_R$ in the 0.4–0.6 range for the states of the $[(\pi h_{9/2})(\nu i_{13/2})^{-1}]$ configuration in ^{196,198}Tl. On the basis of such fragmentary information, there is clearly very little one can say about the $g_K - g_R$ values to be expected for the high-K bands (of uncertain intrinsic configuration) we have postulated above, except that it is plausible that they may be of order unity.

In summary, our speculation concerning the widespread existence throughout the transitional $A \simeq 200$ region of strongly coupled rotational bands associated with high-K, few-quasiparticle states is qualitatively consistent with all aspects of the ob-

served x-ray multiplicity systematics, and is plausible in the light of known spectroscopic properties of lower-spin states.

C. Limitations of the x-ray multiplicity method

We have pointed out earlier (see Secs. II–IV and Ref. 12) a number of important advantages over more traditional techniques that the x-ray multiplicity method (XMM) has in determining absolute evaporation-residue cross sections for the systems we have studied. Before attempting to extend this method to different projectile-target combinations, it is important to understand two significant limitations on its applicability. First, in the prompt x-ray spectrum at least one of the Z_{CN} K x-ray peaks must be well resolved from, and not swamped by background due to, the other x-ray peaks present in the spectrum. Second, the average multiplicity $\langle M_K \rangle$ must be high enough ($\gtrsim 1$), and must vary sufficiently slowly from one residual isotope to another, that the assumption of a Poisson multiplicity distribution is a good approximation to reality.

The first condition makes it difficult, for example, to apply XMM to reactions induced by Be or B projectiles, since K_β peaks from elements of lower Z (see Sect. III B) will then usually interfere with the K_α peaks characteristic of Z_{CN}. This should be less of a problem for still heavier projectiles, where the Z_{CN} K_α peaks will emerge on the high-energy side of the intense K_β region for targetlike products. In Li-induced reactions on targets with $Z < 70$, the large target x-ray production cross sections (which, at the Li bombarding energies considered here, increase rapidly with decreasing Z of the target) hinder an accurate determination of the area under the Z_{CN} $K_{\alpha 1}$ peak [e.g., the intensity of the target $K_{\beta 1,3}$ peak in the singles spectrum for ^{6}Li+^{165}Ho at $E_{^{6}\mathrm{Li}} = 95$ MeV is ~ 25 times larger than that of the neighboring $K_{\alpha 1}(Z_{CN})$ peak]. A further complication arises from the fact that the energy separation between the Z_{CN} $K_{\alpha 1}$ peak and the target $K_{\beta 1,3}$ decreases with Z of the target from 3.3 keV for Pb to 2.2 keV for Ta and only 1.0 keV for Eu. While these factors make precise evaluation of the x-ray spectra from targets in the rare-earth region more difficult, the analysis would still be possible with a special peak-fitting program, incorporating the measured detector response function for monoenergetic photons and the expected intensity ratios and energy separations between K_α and K_β peaks from the various relevant elements.

The second, more fundamental, limitation on XMM originates in the restrictions imposed by the assumption of a Poisson distribution of M_K values around the mean value (i.e., $\Delta_K{}^2 / \langle M_K \rangle = 1$), under which Eq. (4) for x-ray–x-ray coincidences has been derived. In assessing the limits of the validity of this assumption, we need to consider the statistical properties of the x-ray multiplicity distribution arising from any one γ-decay path, and then the effects of averaging over a number of such distributions associated with different decay paths, each having in general a different mean value. These statistical considerations are described in detail in the Appendix. Taken together with the nuclear structure conditions which ensure a high x-ray multiplicity, as discussed in the preceding subsection, the arguments in the Appendix suggest that the transitional mass region investigated in the present work may well be the optimum region for application of XMM. However, it certainly seems worthwhile to survey x-ray–x-ray coincidence yields, probably with projectiles other than ^{6,7}Li, for other mass and spin regions where mild deformations may be expected.

VI. CONCLUSIONS

The measurement of prompt K x-ray multiplicities for a number of nuclei around $A = 200$ has been presented as a new and useful technique in the investigation of the decay modes of fusion residues. We have applied this technique to determine absolute cross sections for (Li,xn) reaction products at bombarding energies between 55 and 124 MeV. We have furthermore deduced new information concerning the multipolarities of γ transitions deexciting these evaporation residues, complementing data obtained using more conventional spectroscopic methods. In particular, the high x-ray multiplicities observed in the present work ($1 \lesssim \langle M_K \rangle \lesssim 3$) suggest that highly converting, low-energy $M1$ transitions constitute a substantial portion of the γ-decay cascades, especially at moderately high spin ($12 \lesssim I \lesssim 20$), in a large number of nuclides in the transitional region between the shell closure at $N = 126$ and the strongly deformed rare earths. From the unexpectedly simple systematic variation of the $\langle M_K \rangle$ measurements with neutron number within this mass region, we have surmised that the converting transitions occur predominantly among members of mildly deformed, high-K, deformation-aligned rotational bands.

Such structure information can be deduced only

qualitatively and indirectly from the x-ray—x-ray coincidence measurements we have described. It is nonetheless of considerable value because insight into average features of nuclear level schemes is not so easily accessible with other experimental methods in this transitional mass region, where level densities are quite high and γ-decay intensities are usually fragmented among numerous parallel paths. Thus, while some strongly coupled rotational bands, similar to those we have postulated, are already known for a few specific $A \simeq 200$ nuclides from extensive γ-ray spectroscopy, the known bands cannot account for the major portion of the observed x-ray multiplicity.

Further theoretical and experimental work would be useful to assess the validity of our speculations on the structure of the transitional nuclei. For example, it would be interesting to see whether structure calculations using various nuclear models could account for the observed constancy of $\langle M_K \rangle$ in the $N = 110-120$ region, where presently only fragmentary structure predictions exist. Detailed experimental verification of our hypothesis concerning the widespread existence in this region of strongly coupled rotational bands associated with high-K, few-quasiparticle states would require a very extensive program of mapping out level schemes via $\gamma-\gamma$ and x-ray$-\gamma$ coincidence measurements. Hopefully, one could provide sufficient evidence to support or reject the proposed nuclear structure scenario by combining such detailed spectroscopic information for a few selected nuclides with the present systematics of $\langle M_K \rangle$ vs N. Measurements of L x-ray$-K$ x-ray coincidence yields might also shed new light on the energy of the converting transitions, since conversion probabilities vary much more rapidly with energy for L-shell than for K-shell electrons (see Fig. 10). Finally, although we expect that the combination of nuclear structure conditions necessary for high K x-ray multiplicity is probably satisfied better for the $N = 110-120$ nuclides investigated here than for any other mass region, it would still be worthwhile to survey K x-ray$-K$ x-ray coincidence yields for other regions of transitional-shape nuclei.

ACKNOWLEDGMENTS

We are grateful to Dr. D. Friesel for assistance in operating the intrinsic germanium detectors and in delivering the variety of Li beams used in the experiment, and to Dr. G. Emery for helpful discussions of various aspects of x-ray production. One of us (H.J.K.) acknowledges support from the Polish-American Maria Sklodowska-Curie Fund. Our work has been supported in part by the National Science Foundation.

APPENDIX: Statistical Characteristics of the K x-ray Multiplicity Distribution

In Sec. II we showed that the general relationship between the measured doubles-to-singles ratio D for K x-ray$-K$ x-ray (x-x) coincidences and the mean K x-ray multiplicity $\langle M_K \rangle$ depends on the variance $\Delta_K{}^2$ of the multiplicity distribution

$$D \equiv \frac{N_{12}}{N_1 \eta_2} = \langle M_K \rangle + \frac{\Delta_K{}^2}{\langle M_K \rangle} - 1 \ . \tag{A1}$$

In the present work values of $\langle M_K \rangle$ have been extracted from Eq. (A1) under the simplifying assumption that $\Delta_K{}^2 = \langle M_K \rangle$, as would be the case if the probability that M_K x rays are emitted in any single (Li,xn) event varied with M_K according to a Poisson distribution. The validity of this assumption has been verified quantitatively via x-γ coincidence measurements for two of the targets studied, at a single bombarding energy. Can one consider the assumption equally valid for other cases, in which we have not explicitly performed cross-check experiments?

In this Appendix, we present detailed statistical arguments concerning multiple internal conversion which allow us to estimate the extent of possible deviations from a Poisson multiplicity distribution and to assess the consequent practical limits on the validity of the x-x coincidence method for determining absolute evaporation-residue cross sections. These arguments do not require detailed knowledge of the structure of specific nuclides or of the nature of the converting transitions. We suggest, in particular, that the applicability of the Poisson assumption results from two competing tendencies: The distribution characterizing *any one* γ-decay path in a given residual nuclide *must be narrower* than a Poisson distribution with the same mean $\langle M_K \rangle$, while the effect of averaging distributions with different means, as are likely to arise from different decay paths and nuclides, is to *increase* $\Delta_K{}^2/\langle M_K \rangle$.

Let us first consider a single γ-decay path comprising N transitions, the ith of which has a K x-ray emission probability p_i somewhere in the range from 0 to $\beta_{K_{\max}} \leq 1$. The p_i are understood to incorporate the probabilities of both K-shell conver-

sion (as opposed to γ-decay or higher-shell conversion) in the nuclear transitions and radiative (as opposed to Auger) atomic transitions. Since the nuclear transition lifetimes are typically much longer than the atomic K-vacancy lifetimes, it is valid to treat internal conversion from different nuclear transitions in the cascade as independent random processes. The overall K x-ray multiplicity distribution from such a cascade therefore has a mean which is the sum of the individual probabilities,

$$\langle M_K \rangle = \sum_{i=1}^{N} p_i \ , \tag{A2}$$

and a variance which is the sum of the individual variances,

$$\Delta_K{}^2 = \sum_{i=1}^{N} p_i(1-p_i) \ . \tag{A3}$$

For a given value of $\langle M_K \rangle$, the *broadest* possible multiplicity distribution from a single decay path arises when the x-ray emission is uniformly distributed over all N transitions in the cascade; we then have a simple binomial distribution with

$$\begin{aligned} p_i &= p = \langle M_K \rangle N^{-1} \ , \\ \Delta_K{}^2 &= \langle M_K \rangle (1-p) \ , \\ D &= \langle M_K \rangle (1-N^{-1}) \ . \end{aligned} \tag{A4}$$

For such a distribution the doubles-to-singles ratio D would underestimate $\langle M_K \rangle$ by $\sim 5-10\%$, since typically $N \sim 10-20$ in the spin region of interest in the present work.

A more serious underestimate of $\langle M_K \rangle$ would result from a single decay path if the conversion probability were concentrated among significantly *fewer* than N transitions. For a given measured value of D the *narrowest conceivable* distribution corresponds to $N_{\min}$ converting transitions, all but one of which are maximally converting ($p_i = \beta_{K_{\max}}$), the remaining transition having a K x-ray emission probability p' appropriate to reproduce D. Equations (A1)–(A3) yield the following characteristics of such a distribution:

$$N_{\min} = [2 + D/\beta_{K_{\max}}] \ , \tag{A5}$$

(where the square brackets signify truncation of the contents to the nearest smaller integer);

$$p' = \frac{(N_{\min}-1)\beta_{K_{\max}}\{D-(N_{\min}-2)\beta_{K_{\max}}\}}{\{2(N_{\min}-1)\beta_{K_{\max}}-D\}} \ , \tag{A6}$$

$$\langle M_K \rangle = (N_{\min}-1)\beta_{K_{\max}} + p' \ , \tag{A7}$$

$$\Delta_K{}^2 = (N_{\min}-1)\beta_{K_{\max}}(1-\beta_{K_{\max}}) + p'(1-p') \ . \tag{A8}$$

This distribution gives rise to the "worst-case"

TABLE II. Possible underestimates of $\langle M_K \rangle$ from x-x coincidences for a single γ-decay path.

D[a]	$N_{\min}$[b]	$\left[\frac{\Delta_K{}^2}{\langle M_K \rangle}\right]_{\min}$[b]	$\left[\frac{D}{\langle M_K \rangle}\right]_{\min}$[b] (worst case)	$\left[\frac{D}{\langle M_K \rangle}\right]_{\text{lower}}$[c] (practical limit)
0.5	2	0.41	0.46	0.75
1.0	3	0.37	0.61	0.83
1.5	4	0.32	0.69	0.88
2.0	4	0.33	0.75	0.88
2.5	5	0.34	0.79	0.90
3.0	6	0.33	0.81	0.92
3.5	7	0.30	0.83	0.93

[a]The x-ray doubles-to-singles ratio, see Eq. (A1).
[b]Values calculated from Eqs. (A5)–(A8) for the narrowest conceivable multiplicity distribution consistent with the specified value of D. The maximum possible probability of K x-ray emission from any one transition is taken to be 0.70, and consequently $\Delta_K{}^2/\langle M_K \rangle \geq 0.30$.
[c]The practical lower limit on $D/\langle M_K \rangle$ assumes a binomial distribution with $2N_{\min}$ transitions.

lower limit values of the ratio $D/\langle M_K\rangle$ specified in Table II for various values of D, evaluated for $\beta_{K_{max}}=0.7$. The latter value represents the maximum internal conversion K x-ray emission probability for $E2$ or $M1$ transitions (of any energy) in the $Z=80$ region (see Fig. 10).

Even under the extreme assumption that the (Li,xn) reaction for a given target and bombarding energy leads predominantly to a single γ cascade, it is highly unlikely that the corresponding x-ray multiplicity distribution could be systematically as narrow as the worst-case distribution considered above. If so few converting transitions were actually involved, one would expect large fluctuations in $\langle M_K\rangle$ from one isotope to the next, and hence a rapid variation with bombarding energy, in marked contrast to the observations (see Fig. 11 and Ref. 12). In our estimate of systematic errors in σ_{xn}, we have based *practical* lower limits on $D/\langle M_K\rangle$ (see Table II) on binomial distributions involving *twice* the minimum possible number of transitions (i.e., $2N_{min}$). The mean K x-ray emission probability for such binomial distributions is typically $p=0.2-0.3$, values quite consistent, for example, with average conversion coefficients for transitions among states of the known low-lying strongly coupled rotational bands in the neutron-poor Tl isotopes.[33,35] For the range of D values measured in the present work ($D\geq 0.8$), we conclude from these arguments that $\langle M_K\rangle$ may be underestimated, and hence σ_{xn} from Eq. (11) overestimated, by at most 10–20%.

In reality, of course, a number of γ cascades in several residual nuclides must participate with appreciable probability in the (Li,xn) reaction for a given target and bombarding energy. Different decay paths will be characterized in general by individual x-ray multiplicity distributions with different mean values and widths. The observed x rays result from an overall distribution averaged over all these decay paths. The averaged distribution tends to be *broader* than its constituents, as can be illustrated by considering the averaging of two binomial distributions with the same single-chance emission probabilities p. Suppose that the first distribution has a mean value $\langle M_K\rangle_1$ arising from N_1 transitions ($N_1=\langle M_K\rangle_1/p$), and is weighted by a probability A_1 [i.e., the fraction A_1 of all (Li,xn) events are characterized by this distribution]; the second distribution has $\langle M_K\rangle_2=f\langle M_K\rangle_1$, $N_2=fN_1$ (with $f>1$), and a weight $A_2=1-A_1$. The averaged distribution (which is *not* itself binomial) then has:

$$\langle M_K\rangle=\langle M_K\rangle_1(A_1+A_2f)\,, \tag{A9}$$

$$\Delta_K{}^2/\langle M_K\rangle=(1-p)+\langle M_K\rangle A_1A_2(f-1)^2/(A_1+A_2f)^2\,, \tag{A10}$$

$$D/\langle M_K\rangle=\frac{A_2(f-1)\{N_1(f+1)-1\}+(N_1-1)}{N_1\{A_2(f-1)+1\}^2}\,. \tag{A11}$$

It is clear from Eq. (A10) that the width $\Delta_K{}^2/\langle M_K\rangle$ of the averaged distribution is *always* greater than the width $(1-p)$ of the constituent distributions. For given values of f and N_1 the distribution broadening is *maximized* when

$$A_2=\{N_1+(f-1)^{-1}\}/\{N_1(f+1)-1\}\,, \tag{A12}$$

$$(D/\langle M_K\rangle)_{max}=(f+1-N_1{}^{-1})^2/4f\,. \tag{A13}$$

It can be shown that if one were now to average in *additional* binomial distributions (at the expense of the probabilities A_1 and A_2), with single-chance probabilities p and mean values differing from $\langle M_K\rangle_1$ by factors f_i', $1<f_i'<f$, the resultant distribution would always be broader than the constituents but *not as broad* as in the two-binomial case represented by Eqs. (A12) and (A13).

A practical *upper* limit on $D/\langle M_K\rangle$ can therefore be based on Eq. (A13), using estimated maximum values for N_1 ($N_{1_{max}}\simeq 20$ transitions) and for the ratio f between the means of constituent distributions which contribute significantly to the overall x-ray multiplicity distribution. As discussed in Ref. 12 and Sec. V B, the consistency of the x-γ coincidence results for neighboring (Li,xn) residues, and the absence of any strong fluctuations in $\langle M_K\rangle$ with bombarding energy or neutron excess of the populated residues, all suggest that $f_{max}\simeq 2$ is a conservative estimate for those cases in which $D\gtrsim 2$. In those cases (e.g., ^{6}Li+^{181}Ta) where D is close to 1.0, and the measurement uncertainties in D are usually larger than for the other targets, a somewhat larger value of f_{max} is possible. From these considerations and Eq. (A13) we conclude that

$\langle M_K \rangle$ may be *overestimated,* and hence σ_{xn} *underestimated,* in the present work by at most 10–20%.

All of the quantitative conclusions from the statistical arguments presented here are well incorporated by assigning a possible systematic error of ± 0.2 to the $\langle M_K \rangle$ values deduced from our x-ray–x-ray coincidence measurements. It is conceivable that the Poisson assumption would remain reasonably valid even if the number of relevant transitions in any one decay path were significantly smaller than we have assumed here, since then one would expect larger fluctuations in $\langle M_K \rangle$ between different paths and nuclides (i.e., larger $f_{\max}$), and hence greater distribution broadening. Nonetheless, if the measured values of D were significantly smaller than unity or if they exhibited strong isotopic variations among the xn residues, it would be difficult to assess the quantitative validity of the x-x coincidence method without much more detailed nuclear structure information.

---

*On leave from Institute of Nuclear Research, Swierk, Poland.
†Present address: Bhabha Atomic Research Centre, Bombay, India.
‡Present address: Institute for Nuclear Studies, Tokyo, Japan.
§Present address: Physics Department, California Institute of Technology, Pasadena, California.
||Present address: Physics Department, Massachusetts Institute of Technology, Cambridge, Massachusetts.

[1]W. E. Meyerhof and K. Taulbjerg, Annu. Rev. Nucl. Sci. 27, 279 (1977).
[2]J. Smolorz, S. Hoppenau, S. Röhl, W. A. Schönfeldt, and M. Dost, Phys. Rev. A 21, 207 (1980).
[3]V. Zoran, A. Berinde, C. Deberth, M. Dost, I. Neamu, C. Protop, S. Röhl, and N. Scintei, J. Phys. G 6, 117 (1980).
[4]Z. Sujkowski, D. Chmielewska, R. V. F. Janssens, and M. J. A. de Voigt, Phys. Rev. Lett. 43, 998 (1979); D. Chmielewska, Z. Sujkowski, R. V. F. Janssens, and M. J. A. de Voigt, Nucl. Phys. A366, 142 (1981).
[5]R. Anholt, Phys. Lett. 88B, 262 (1979); W. E. Meyerhof, R. Anholt, and W. Wölfli, *ibid.* 84B, 59 (1979).
[6]J. S. Blair, P. Dyer, K. A. Snover, and T. R. Trainor, Phys. Rev. Lett. 41, 1712 (1978).
[7]S. M. Shafroth, J. Franklin Inst. 298, 339 (1974).
[8]S. Röhl, S. Hoppenau, and M. Dost, Phys. Rev. Lett. 43, 1300 (1979); M. Dost, S. Hoppenau, J. Kising, S. Röhl, and P. Schorn, Phys. Rev. A 24, 693 (1981).
[9]G. Deconninck and N. Longequeue, Phys. Rev. Lett. 30, 863 (1973).
[10]G. Deconninck and M. Longrée, Phys. Rev. A 16, 1390 (1977).
[11]S. S. Kapoor, S. K. Kataria, S. R. S. Murthy, D. M. Nadkarni, V. S. Ramamurthy and P. N. Rama Rao, Phys. Rev. C 4, 2165 (1971); W. Reisdorf, J. P. Unik, M. C. Griffin, and L. E. Glendenin, Nucl. Phys. A177, 337 (1971).
[12]H. J. Karwowski, S. E. Vigdor, W. W. Jacobs, S. Kailas, P. P. Singh, F. Soga, and W. Ploughe, Phys. Rev. Lett. 42, 1732 (1979).
[13]H. J. Karwowski, S. E. Vigdor, W. W. Jacobs, T. G. Throwe, D. L. Wark, S. Kailas, P. P. Singh, F. Soga, T. E. Ward, and J. Wiggins, Phys. Rev. Lett. 47, 1251 (1981).
[14]S. E. Vigdor, H. J. Karwowski, W. W. Jacobs, S. Kailas, P. P. Singh, F. Soga, and T. G. Throwe, report, 1982, S. E. Vigdor, Nukleonika (to be published).
[15]J. H. Scofield, Phys. Rev. A 9, 1041 (1974).
[16]G. T. Emery in *Atomic Inner Shell Processes,* edited by B. Crasemann (Academic, New York, 1975), Vol. I, p. 202, and references therein.
[17]G. B. Hagemann, R. Broda, B. Herskind, M. Ishihara, S. Ogaza, and H. Ryde, Nucl. Phys. A245, 166 (1975); P. O. Tjøm, F. S. Stephens, R. M. Diamond, J. de Boer, and W. E. Meyerhof, Phys. Rev. Lett. 33, 593 (1974).
[18]J. H. Scofield in *Atomic Inner Shell Processes,* edited by B. Crasemann (Academic, New York, 1975), Vol. I, p. 265.
[19]P. Schwandt, (private communication).
[20]W. W. Jacobs, H. J. Karwowski, S. E. Vigdor, and T. G. Throwe (unpublished).
[21]T. L. Hardt and R. L. Watson, Phys. Rev. A 7, 1917 (1973).
[22]J. D. Garcia, R. J. Fortner, and T. M. Kavanagh, Rev. Mod. Phys. 45, 111 (1973).
[23]W. Rubinson, Phys. Rev. 130, 2041 (1963).
[24]T. Åberg in *Atomic Inner Shell Processes,* edited by B. Crasemann (Academic, New York, 1975), Vol. I, p. 353, and references therein.
[25]*Table of Isotopes,* 7th ed., edited by C. M. Lederer and V. S. Shirley (Wiley, New York, 1978).
[26]R. S. Hager and E. C. Seltzer, Nucl. Data A4, 1 (1968).
[27]R. M. Diamond and F. S. Stephens, Annu. Rev. Nucl. Sci. 30, 89 (1980) and references therein.
[28]R. S. Simon, M. V. Banaschik, R. M. Diamond, J. O. Newton, and F. S. Stephens, Nucl. Phys. A290, 253 (1977); M. A. Deleplanque, T. Byrski, R. M. Diamond, H. Hübel, F. S. Stephens, B. Herskind, and B. Bauer, Phys. Rev. Lett. 41, 1105 (1978); M. A. Deleplanque, J. P. Husson, N. Perrin, F. S. Stephens, G. Bastin, C. Schück, J. P. Thibaud, L. Hildingsson, S. Hjørth, A. Johnson, and T. Lindblad, *ibid.* 43, 1001 (1979).
[29]J. O. Newton and S. H. Sie, Nucl. Phys. A334, 499 (1980).

[30]H. Hübel, R. M. Diamond, F. S. Stephens, B. Herskind, and R. Bauer, Z. Phys. A 297, 237 (1980).
[31]J. P. Vivien, Y. Schutz, F. A. Beck, E. Bozek, T. Byrski, C. Gehringer, and J. C. Merdinger, Phys. Lett. 85B, 325 (1979).
[32]S. J. Feenstra, J. V. Klinken, Y. P. Pijn, R. Janssens, C. Michel, J. Steyaert, J. Vervier, K. Cornelis, M. Huyse, and G. Lhersonneau, Phys. Lett. 80B, 183 (1979); L. Westerberg, D. G. Sarantites, K. Geoffroy, R. A. Dayras, J. R. Beene, M. L. Halbert, D. C. Hensley, and J. H. Barker, Phys. Rev. Lett. 41, 96 (1978).
[33]R. M. Lieder, A. Neskakis, M. Müller-Veggian, V. Gono, C. Meyer-Böricke, S. Beshai, F. Fransson, G. G. Linden, and T. Lindblad, Nucl. Phys. A299, 255 (1978).
[34]F. S. Stephens in *Elementary Modes of Excitation in Nuclei,* edited by A. Bohr and R. A. Broglia (North-Holland, Amsterdam, 1977), p. 172.
[35]A. J. Kreiner, M. Fenzl, and W. Kutschera, Nucl. Phys. A308, 147 (1978); A. J. Kreiner, M. Fenzl, S. Lunardi, and M. A. J. Mariscotti, *ibid.* A282, 243 (1977); A. J. Kreiner, M. Fenzl, U. Heim, and W. Kutschera, Phys. Rev. C 20, 2205 (1979).
[36]D. Proetel, R. M. Diamond, and F. S. Stephens, Nucl. Phys. A231, 301 (1974).
[37]H. Hübel, A. Kleinrahm, C. Günther, D. Mertin, and R. Tischler, Nucl. Phys. A294, 177 (1978); B. V. Thirumala Rao, R. Broda, C. Günther, A. Kleinrahm, and M. Ogawa, *ibid.* A362, 71 (1981).
[38]J. Kropp, H. Klewe-Nebenius, H. Faust, J. Buschmann, H. Rebel, H. J. Gils, and K. Wisshak, Z. Phys. A 280, 61 (1977).
[39]The transitional nuclei tend to be somewhat triaxial in shape (see Refs. 33 and 34) and thus should not be expected to adhere strictly to Eqs. (12) and (13). Nonetheless these simple collective-model relations are adequate for indicating the qualitative conditions necessary for $M1$ enhancement, and may even provide a reasonable quantitative description for average properties of such strongly coupled bands, as would be sampled by the x-ray multiplicity measurements.
[40]A. Bohr and B. R. Mottelson, *Nuclear Structure* (Benjamin, Reading, Mass., 1975), Vol. II.
[41]H. Morinaga and T. Yamazaki, *In-Beam γ-Ray Spectroscopy* (North-Holland, Amsterdam, 1976).
[42]A. J. Kreiner, M. A. J. Mariscotti, C. Baktash, E. der Mateosian, and P. Thieberger, Phys. Rev. C 23, 748 (1981).
[43]J. O. Newton, F. S. Stephens, and R. M. Diamond, Nucl. Phys. A236, 225 (1974); J. O. Newton, S. D. Cirilov, F. S. Stephens, and R. M. Diamond, *ibid.* A148, 593 (1970).
[44]H. Toki, H. L. Yadav, and A. Faessler, Z. Phys. A 292, 79 (1979).
[45]O. Prior, F. Boehm, and S. G. Nilsson, Nucl. Phys. A110, 257 (1968).
[46]I-L. Lamm, Nucl. Phys. A125, 504 (1969).
[47]K. S. Krane, At. Data Nucl. Data Tables 18, 137 (1976); 25, 29 (1980).
[48]M. G. Slocombe, J. O. Newton, and G. D. Dracoulis, Nucl. Phys. A275, 166 (1977).